Manuscript prepared for Nat. Hazards Earth Syst. Sci.
with version 2014/09/16 7.15 Copernicus papers of the LaTeX class copernicus.cls.
Date: 13 June 2015

Landslide susceptibility mapping in the Mawat area, Kurdistan Region, NE Iraq: a comparison of different statistical models

A. A. Othman[1,2,3], R. Gloaguen[1,3], L. Andreani[1,3], and M. Rahnama[1,3]

[1]Remote Sensing Group, Institute of Geology, TU Bergakademie Freiberg, B.–von–Cotta–St. 2, D-09596 Freiberg, Germany
[2]Iraq Geological Survey, Al–Andalus Square, Baghdad, Iraq
[3]Remote Sensing Group, Helmholtz Institute Freiberg of Resource Technology, Halsbrueckerstr. 34, D-09599 Freiberg, Germany

Correspondence to: A. A. Othman (arsalan-ahmed.othman@student.tu-freiberg.de)

Abstract. During the last decades, expansion of settlements into areas prone to landslides in Iraq has increased the importance of accurate hazard assessment. Susceptibility mapping provides information about hazardous locations and thus helps to potentially prevent infrastructure damage due to mass wasting. The aim of this study is to evaluate and compare frequency ratio (FR), weight of evidence (WOE), logistic regression (LR) and probit regression (PR) approaches in combination with geomorphological indices to determine the landslide susceptibility (LS). We tested these four methods in the Mawat area, Kurdistan Region, NE Iraq, where landslides occur frequently. For this purpose, we evaluated 16 geomorphological, geological and environmental predicting factors mainly derived from the advanced spaceborne thermal emission and reflection radiometer (ASTER) satellite. The available reference inventory includes 351 landslides representing a cumulative surface of 3.127 km^2. This reference inventory was mapped from QuickBird data by manual delineation and partly verified by field survey. The areas under the curve (AUC) of the Success Rate Curve (SRC), and relative landslide density (R index) show that all models perform similarly and that focus should be put on the careful selection of proxies. In order to estimate models uncertainties, we produced 50 landslide susceptibility maps for each approach using the same thematic information but different landslide training dataset (bootstrap aggregating). These landslide susceptibility maps are exploited to determine the error associated with the susceptibility assessment and the sensitivity for the four compared approaches. The results show that the FR has less errors and less variability. The results indicate that lithology and slope aspects are the dominant factors leading to the occurrence of landslides. Furthermore, this paper demonstrates that using hypsometric integral as a prediction factor instead of slope curvature gives better results and increases the accuracy of the LS.

1 Introduction

Mass movements such as landslides are one of the most damaging natural hazards since they affect several social and economic aspects. They represent a major risk to human life, as well as private and public properties (Calo et al., 2014; Petley, 2012). Maps of landslides are classified into three classes: inventory maps, density maps, and hazard maps (Guzzetti et al., 2000). Moreover, landslide investigations can be categorized into three main groups: (1) landslide recognition, classification, and post-event analysis, (2) landslide monitoring, and (3) landslide susceptibility and hazard assessment (Scaioni et al., 2014; Mantovani et al., 1996; Metternicht et al., 2005).

Landslide inventory maps represent the spatial distribution of deposition (accumulation) and depletion zones produced by a gravity-induced mass movement, which may vary in type, age, and activity (Guzzetti et al., 1999). A landslide inventory map can be prepared by different techniques (Guzzetti, 2006). Until now, visual interpretation of aerial photographs and high spatial resolution images in combination with field validation is the most prominent and accurate technique for the preparation of landslide inventory maps (Othman and Gloaguen, 2013a). The landslide inventory map is a fundamental basis to derive the landslide susceptibility (LS) map (Zhao et al., 2012), which is defined as the probability of the terrain to trigger a landslide over a set of geo-environmental conditions (Ozdemir and Altural, 2013). Such maps are essential for the estimation of landslide prone areas (Guzzetti et al., 2005). In addition, the LS is a fundamental and very useful tool supporting decision making in the field of land use management and planning (Akgun, 2012).

Over the last decades, many susceptibility estimation techniques have been implemented for the LS estimation. These techniques include frequency ratio (FR) (Ozdemir and Altural, 2013; Lee and Talib, 2005; Shahabi et al., 2014), weight of evidence (WoE) (Ozdemir and Altural, 2013; Lee, 2013; Lee et al., 2002a; Tseng et al., 2015), analytical hierarchy process (Shahabi et al., 2014; Ayalew et al., 2005), bivariate statistical analyzes (Ayalew et al., 2005; Althuwaynee et al., 2014), artificial neural networks (Lee et al., 2001; Conforti et al., 2014; Qiao et al., 2013; Ercanoglu, 2005; García-Rodríguez and Malpica, 2010), support vector machines (Yao et al., 2008; Peng et al., 2014), and logistic regression (LR) (Ozdemir and Altural, 2013; Shahabi et al., 2014; Lee and Min, 2001; Atkinson and Massari, 1998). All these prediction techniques are based on the popular assumption that "the past and the present landslide locations are the key to the future" (Carrara et al., 1995; Capitani et al., 2013a; Zezere, 2002; Van Den Eeckhaut et al., 2006). In other words, slope failures are determined by controlling factors, and future slope failures will occur under the same conditions as past slope failures (Lee and Talib, 2005). Under this assumption, a set of factors which controlled past landslides can be used to predict future occurrences of landslides.

Therefore, estimation and statistical analysis of the relationship between the predicting factors for landslides and the occurrences of landslides helps to deepen our conceptual knowledge of LS techniques which will help to develop more sophisticated and more accurate techniques in the future (Carrara et al., 1995; Capitani et al., 2013a; Van Den Eeckhaut et al., 2006). So far, lithology, slope

gradient, slope aspect, distance to streams, and to tectonic lineaments are widely accepted as significant factors that are related to the occurrence of landslides (Ozdemir and Altural, 2013; Capitani et al., 2013a; Kayastha et al., 2013; Wang et al., 2013).

In this study, we produced LS maps for a part of the Iraqi Zagros mountain belt, where no LS studies have been carried out yet. We selected 16 predicting factors, which play a dominant role in slope stability. These factors are (1) lithology, (2) land cover, (3) slope gradient, (4) slope aspect, (5) slope curvature, (6) plan curvature, (7) profile curvature, (8) the hypsometric integral, (9) elevation, (10) drainage density, (11) distance to drainage, (12) distance to lineaments, (13) precipitation, (14) normalized difference vegetation index (NDVI), (15) topographic position index (TPI) and (16) topographic wetness index (TWI).

We apply a variety of GIS techniques such as raster calculation, raster to vector conversion, vector to raster conversion, and overlay to compare the four landslide susceptibility models (FR, WOE, LR and PR) and to evaluate their performances regarding the estimation of the landslide probability. The PR is also applied for the first time to model LS.

This study is organized in four main steps: (1) preparation of a landslide inventory map based on QuickBird imagery interpretation, without any consideration of time of occurrences, (2) determination of predicting factors for landslides, (3) Modelization of LS using four models, and (4) performing statistical comparisons between the four examined models.

2 Study area

2.1 Location

The study area is located between 35°45′ and 36°00′ N and between 45°26′ and 45°35′ E. It comprises the Iraq Zagros Mountains, where mass movements threaten many villages and towns (Othman and Gloaguen, 2013a, b). The studied area covers about 422 km^2, and encompasses parts of the Sulaimaniyah Governorate/Kurdistan Region in NE Iraq (Fig. 1). The global landslide hazard distribution map (CHRR et al., 2005) suggests medium to high risk of landslide occurrence there.

2.2 Geological setting

The Zagros orogenic belt is a part of the Alpine-Himalayan mountain ranges and trends in NW–SE direction. This belt is approximately 2000 km long, extending from SE Turkey through Iraq to southern Iran (Alavi, 1994, 2004). The Iraqi part of the Zagros orogenic belt consists of three main tectonic zones: (1) the Inner Platform (stable shelf), (2) the Outer Platform (unstable shelf), which comprises the Mesopotamia Foredeep, the Foothill Zone, the High Folded Zone, and the Imbricated Zone (IZ), and (3) the Zagros Suture Zone (ZSZ) (Fouad, 2010; Agard et al., 2011; Lawa et al., 2013; Jassim and Goff, 2006 ;Fig. 1).

Most of the study area lies within the ZSZ, represented by the Penjween-Walash Zone (PWZ), the Qulqula-Khwarkurk Zone (QKZ), and a small part of the Arabian Outer Platform (unstable shelf) represented by the IZ (Fig. 1). The PWZ is located in the central part of the study area. It consists of ultramafics, gabbro, metabasalt, conglomerates, sandstones, marbles, calc-schists, volcanic basalt and andesite. The QKZ is located in the northeastern part of the study area. It consists of radiolarian mudstone, chert, limestone and pebbly conglomerate rocks. The IZ is located in the southwestern part of the study area. It includes three formations, which are composed mainly of limestones, calcareous sandstones, marls, mudstones, shales, and conglomerates. Two main thrust faults clearly mark the upper and lower contacts of the PWZ. The two thrusted sheets have steep slopes, folds of chevron type, and contain boudinage structure. The area formed during the Late Cretaceous and Mio-Pliocene periods (Jassim and Goff, 2006; Smirnov and Nelidov, 1962; Al-Mehaidi, 1974; Buday and Suk, 1978; Ma'ala, 2008).

2.3 Climate

The Mawat area is characterized by annual variations in precipitation, temperature and evaporation. It has dry summers and wet winters (Fig. 2). The bulk of annual precipitation ($896\,\mathrm{mm}$) occurs from October to May. The highest precipitation amounts are received in January with an average value of $199.6\,\mathrm{mm/month}$. Monthly temperatures range between $-2.1\,^{\circ}\mathrm{C}$ (January) and $37.3\,^{\circ}\mathrm{C}$ (August). The snowfalls occur for $> 10\,\mathrm{days\,yr^{-1}}$ on average between November and April. Heavy snowfall and rapid snow melting increase the risk of landslides in the Mawat area.

2.4 Landslides

Landslides in the area are frequent and they are mainly due to natural and anthropogenic triggers (Fig. 3). The very rugged topography is reflected by strong variations in slope and altitude. Heavy rainfall and rapid snow melting in spring in combination with heterogeneous geology and geomorphology are the main natural factors controlling the distribution of mass movements. Civil engineering activities like road cuts, overloading of the upper parts of landslides or undercutting of the toe of slopes are the main human-induced factors (Othman and Gloaguen, 2013a; Sissakian et al., 2004).

Landslides have affected large areas along the main road to Gimo Mountain, after Kanaro village. Recent events blocked roads and several nearby towns are regularly threatened and affected. A large rockfall was witnessed recently in the north of Chowarta town (Fig. 3). A huge mass of igneous rock of the Mawat massif has collapsed in the last decade. The roads from Sulimanyah to Mawat are also affected by recurrent translational slides or rockslides of different sizes. Figure(3) shows that slump sliding threatens roads at different sites of the Mawat area. Clastic debris flows are also common in the weak layers (Othman and Gloaguen, 2013a).

Othman and Gloaguen (2013a) used two sources of information to prepare an inventory map in our study area, which includes 351 landslides. The first source is the previous geological map of the

northeast Iraq by Buday and Suk (1978), which has a scale of $1:100\,000$. The second source is QuickBird imagery, which has visually been interpreted and digitized. The inventory map has partly been verified by our own observations during a field survey in different parts of the study area. The landslide boundaries were identified using viewing scale of 1:2500 using QuickBird data. Decision making was based on attributes such as texture, tone, headwall scarps, associations like fragments of transferred materials, and the pathway of these materials. The total landslide coverage accounted for an area of $3{,}127\,\mathrm{km}^2$. The size of detected landslides ranges from $16\,\mathrm{m}^2$ to $0.32\,\mathrm{km}^2$, with a mean area of 10118 m^2. The landslides rate % is 0.741 .

3 Methodology

3.1 Material

The ASTER sensor has 14 bands including Nadir (N) and backward-looking (B) (0.76–0.86 $\mu\mathrm{m}$) for the third band. ASTER scenes cover $60\,\mathrm{km} \times 60\,\mathrm{km}$ on land (Abrams and Hook, 2001). The ASTER level 1A system scene of $15\,\mathrm{m}$ resolution was orthorectified and acquired on 24 August 2003. Moreover, four cloud-free QuickBird scenes were used. The scenes were acquired on 29 August 2006 via Ministry of Planning (Iraq). The scenes were orthorectified, radiometrically corrected, and projected using the WGS84 datum and the UTM 38N projection. The final products are an 8-bit imagery, with $0.6\,\mathrm{m}$ spatial resolution, and comprise three visible spectral bands: blue (0.45 to 0.52 $\mu\mathrm{m}$), green (0.52 to 0.6 $\mu\mathrm{m}$) and red (0.63 to 0.69 $\mu\mathrm{m}$) (DigitalGlobe, 2006).

Satellite data were processed using the ENVI (Environment for Visualizing Images) software. Lineaments were automatically extracted from a Digital Elevation Model (DEM) using TecLines, a MATLAB based toolbox (Rahnama and Gloaguen, 2014b, a). The hypsometric index and the drainage network were extracted using TecDEM, which is also a MATLAB-based toolbox (Shahzad and Gloaguen, 2011). Additional GIS operations (Slope, Aspect, curvature, plan curvature, profile curvature, topographic wetness index, density map, distance map, interpolation and base map), as well as the preparation of final maps were performed using ArcGIS10 (ESRI, 2011). Statistical analyzes were conducted using R-based scripts.

3.2 Input and preparing parameters

There is no agreement on which predictive factors have to be used in LS analyzes, but most studies highlighted the importance of topographical, geological and environmental factors (Nefeslioglu et al., 2008a). Sixteen predictive factors were selected, and stored as thematic maps. These factors were classified into three categories: geomorphological, geological, and environmental. Thematic maps were resampled in order to have the same spatial resolution than the pixel size of ASTER DEM, (i.e. $15\,\mathrm{m}$ spatial resolution).

The input parameters can be discrete and continuous: lithology, land cover and slope aspect (group A) are discrete while the rest (group B) are continuous. We prepared the input parameters in two ways based on the applied model. The first way is used for FR and WOE models while the second one is used for LR and PR models. The FR and WOE models are only able to exploit input parameters that have a discrete form (variables that can take on one of a fixed number of possible values, thus assigning each individual to a particular category; Schicker and Moon, 2012). Therefore, we classified each factor of group B into several classes to be in a discrete form like group A. The LR and PR models are able to exploit input parameters that have discrete or continuous (those variables that are measured in terms of numbers) forms or any combination of both forms (Choi et al., 2012; Atkinson and Massari, 1998), but the discrete form should be binary (zero and one). Therefore, we binarized each parameter of group A. For example, the lithological map shows 9 classes. For each class, a binary map was created that states “one" if an individual lithology is apparent and states “zero" if not. This results in 9 input maps for lithology, one for each lithological class.

3.2.1 Geomorphological factors

In the susceptibility estimation, we used the following eight geomorphological variables: (1) elevation (DEM) which affects the occurrence of landslides and indirectly affects climatic conditions and hence soil erosion (Ozdemir and Altural, 2013; Wang et al., 2013; Xu et al., 2012). The DEM was extracted from Nadir (N) and backward-looking (B) bands of ASTER data. The other geomorphological parameters were extracted from the ASTER DEM. (2) Slope gradient, which is the major factor of slope stability analysis (Lee and Min, 2001; Yalcin et al., 2011). (3) Slope aspect, which is associated to solar radiation, the wind, and rainfall (Yalcin et al., 2011). Hence, slope aspect is assumed to have an impact on vegetation cover and, therefore, may affect the occurrence of landslides (Garcia-Rodriguez et al., 2008). Three types of curvature maps were used: (4) Slope curvature (Nefeslioglu et al., 2008b), (5) Profile curvature and (6) Plan curvature (Moore et al., 1991). For plan, profile, and slope curvatures, a positive value reflects a slope-upwards convex surface of that cell. A negative value refers to a slope-upwards concave surface. A value of 0 refers to a flat surface (Xu et al., 2012; Mancini et al., 2010). These parameters were derived using a 3×3 moving window in standard ArcGIS tools (ESRI, 2012). (7) Hypsometric integral (HI) is an appropriate index to identify the evolutionary stage of landscape development (Othman and Gloaguen, 2013b; Strahler, 1952; Perez-Pena et al., 2009). Only Lin et al. (2011) already explored this index as one of predictive factors when they realized a susceptibility zonation in Taiwan. HI values above 0.6 indicate elevated landscapes with an entrenched drainage network. HI values between 0.35 and 0.6 correspond to significantly eroded areas with a developed system of V-shaped valleys, and values below 0.35 indicate relatively flat landscapes with a low degree of incision (Strahler, 1952). The HI map was computed using a 100 pixels ($\sim 1.5\,\mathrm{km}$) moving window. According to Pike and Wilson

(1971) the HI of a given area can be estimated using the following Eq. (1):

$$\mathrm{HI} = \frac{\mathrm{Elevation}_{\mathrm{mean}} - \mathrm{Elevation}_{\mathrm{minimum}}}{\mathrm{Elevation}_{\mathrm{maximum}} - \mathrm{Elevation}_{\mathrm{minimum}}}. \tag{1}$$

We furthermore use the (8) topographic position index (TPI, Eqs. 2 and 3) as a predictive factor (Costanzo et al., 2012; Vorpahl et al., 2013). It represents the variation between the elevation of a pixel (E_{C}) and the average elevation (E_{A}) around this pixel (De Reu et al., 2013; Weiss, 2001). The number of pixels defining the area around it n_M are set by the kernel-matrix (M). The TPI is calculated using Eqs. (2) and (3) ;De Reu et al., 2013; Weiss, 2001:

$$\mathrm{TPI} = E_{\mathrm{C}} - E_{\mathrm{A}} \tag{2}$$

$$E_{\mathrm{A}} = \frac{1}{n_M} \sum_{i \in m} E_i. \tag{3}$$

Negative TPI values indicate that the central pixel is situated lower than its average surroundings; while positive TPI values indicate that the central pixel is located higher. We implemented a script in the TecDEM toolbox in order to compute the TPI for the studied area. We used a moving window of 100 pixels ($\sim 1.5\,\mathrm{km}$).

3.2.2 Geological factors

Lithological and structural variations affect the strength and stability of materials (Ayalew and Yamagishi, 2005). We thus used two geological factors as input parameters: (1) lithology, and (2) distance to lineaments. The lithological map of the Mawat area includes eight units (Othman and Gloaguen, 2014).

Previous geological maps are inaccurate regarding the location of faults, and several faults were not mapped. Therefore, we mapped the lineaments using TecLines (Rahnama and Gloaguen, 2014b), which allows the extraction of image discontinuities from a DEM. The DEM was resampled to a resolution of $900\,\mathrm{m}$ in order to avoid noisy image discontinuities. The final lineaments were exported to a shape file. We then computed the density of tectonic lineaments and distance to tectonic lineaments, which are frequently used to map landslide susceptibility (Capitani et al., 2013a, b; Choi et al., 2012; Pradhan et al., 2006).

3.2.3 Environmental factors

We used six environmental predictive factors of landslides: land cover, precipitations, normalized difference vegetation index (NDVI), drainage density, distance to drainage and topographic wetness index (TWI). (1) The land cover map (Al-Rubaiay and Al-Dulaimi, 2012) was provided by GEOSURV-Iraq and contains eight classes. (2) We used precipitation data from climatological stations located within and surrounding the study area. The available data spans a period of $7\,\mathrm{years}$ (2000–2006). We averaged annual precipitation from the daily time series data. In order to obtain

a continuous coverage, we interpolated the point-wise precipitation data using an inverse distance weighting (IDW) method. (3) The NDVI is used to characterize the vegetation cover. Increases in landslide frequency is related to the lack of appropriate vegetation cover that stabilizes slopes (Othman and Gloaguen, 2013a; Shahabi et al., 2014). The NDVI was calculated (Rouse et al., 1974) after extraction of the reflectance (ρ) from the digital number (DN) of ASTER VNIR data level 1A.

Because of the positive relationship between landslide area and rivers (Othman and Gloaguen, 2013b) the drainage network can serve as a robust tool to investigate landslides. We calculated (4) the drainage density from the drainage network around the central point within a predetermined radius of 3000 m. Buffers surrounding the drainage network were used to calculate (5) the distance to drainage. (6) Finally, we used the TWI to study spatial scale effects on hydrological processes. It is a landslide predicting factor related to the runoff (Beven and Kirkby, 1979). The TWI was computed using Eq. (4; Beven and Kirkby, 1979)

$$\mathrm{TWI} = \ln \frac{A_\mathrm{S}}{\tan\theta} \tag{4}$$

where θ is the slope angle (°) and A_S is the catchment area (m^2).

3.3 Landslide susceptibility models

The resulting accuracy of the LS mapping depends on the data quality and the mapping model (Chen et al., 2013). In this study, the spatial relationship between landslide locations and each predicting factor for landsliding was derived using the FR, WOE, LR and PR models. The resulting LS maps based on the different models show similarity and are discussed later on.

3.3.1 Frequency ratio (FR)

The FR represents a simple and common model to generate the LS map (Ozdemir and Altural, 2013; Lepore et al., 2012; Lee and Talib, 2005; Shahabi et al., 2014; Park et al., 2013; Mohammady et al., 2012). We assigned a LS value each cell in the study area by implementing the Eqs. (5 and 6); (Wang et al., 2013; Lepore et al., 2012; Regmi et al., 2010).

$$\mathrm{FR}_j = \frac{\mathrm{Al}_i/\mathrm{Al}}{\mathrm{Ac}_i/A} \tag{5}$$

$$\mathrm{LS} = \sum_{j=1}^{n} \mathrm{FR}_j \tag{6}$$

where Al_i is the number of landslides cells of the category (i), Al is the total number of landslides cells, Ac_i is the number of cells of the category (i), A is the number of cells of the study area, FR_j is the FR value for the chosen class of factor j, and n is the total number of factors included in the study (here $n = 15$). Magnitudes of $\mathrm{FR}_j > 1$ mean high probability of landslide occurrence, whereas $\mathrm{FR}_j < 1$ mean low probability of landslide occurrence (Ozdemir and Altural, 2013; Shahabi et al., 2014).

3.3.2 Weight of evidence (WOE)

The Bayesian probability model, known as the WOE is described in detail by Lee et al. (2002b), Regmi et al. (2010) and Meyer et al. (2014). In summary, positive weights (W^+) and negative weights (W^-) are estimated based on the presence or absence of landslides within the area covered by each predicting factors. Weights are computed using the Eqs. (7 and 8); (Van Den Eeckhaut et al., 2009).

$$W^+ = \ln\left[\frac{\mathrm{Al}_i/\mathrm{Al}}{\mathrm{Ac}_i/A_O}\right] \tag{7}$$

$$W^- = \ln\left[\frac{1-(\mathrm{Al}_i/\mathrm{Al})}{1-(\mathrm{Ac}_i/A_O)}\right] \tag{8}$$

where Al_i is the number of landslides cells of the category (i), Al is a total number of landslides cells, Ac_i is the number of cells of the category (i), A_o is the number of cells outside the landslides i.e. number of study area cells minus the total number of landslides cells. The weight contrast (C) represents the difference between the W^+ and W^- (Eq. 9; Mohammady et al., 2012; Meyer et al., 2014), the magnitude of the contrast reflects the overall factor association between predicting factors and landslides (Ozdemir and Altural, 2013; Mohammady et al., 2012; Meyer et al., 2014). Negative and positive contrasts indicate negative and positive spatial correlations, respectively (Ozdemir and Altural, 2013; Corsini et al., 2009). The final probability (P; Eq. 10; Ozdemir and Altural, 2013) for each cell is the sum of the weights of each predicting factor and the prior probability ($P_{\mathrm{p(s)}}$; Eq. 11).

$$C = W^+ - W^- \tag{9}$$

$$P = \exp\left(\sum W^+ + \ln P_{\mathrm{p(s)}}\right) \tag{10}$$

$$P_{\mathrm{p(s)}} = \frac{\text{Number of landslide cells}}{\text{Number of total study area cells}} \tag{11}$$

3.3.3 Logistic regression (LR)

The logistic regression is a multivariate statistical regression analysis. The model has been widely applied for LS mapping (Guzzetti et al., 1999). Results range between one and zero, where one corresponds to the presence and zero to the absence of landslides, respectively (Althuwaynee et al., 2014). The LR model is expressed as Eqs. (12 and 13); (Kleinbaum and Klein, 2011):

$$P = \frac{1}{1+e^{-z}} \tag{12}$$

$$z = \alpha + \beta_1 X_1 + \beta_2 X_2 + \ldots + \beta_n X_n \tag{13}$$

where α is the intercept of the model, n is the number of variables, β are the beta values associated with each of the independent variables, P is the probability which varies between 0 and 1 on an S-shaped curve and z varies from $-\infty$ to $+\infty$ on an S-shaped curve.

3.3.4 Probit regression (PR)

We performed a probit regression, which is a binomial statistical regression. The probit link function represents the inverse of the cumulative distribution function of the standard normal distribution to transform probabilities to the standard normal variable. This model is described by (Eqs. 14 and 15); (Aldrich and Nelson, 1984; McCullagh and Nelder, 1983):

$$z = \Phi^{-1} P \tag{14}$$

$$\Phi(z) = \frac{1}{\sqrt{2\pi}} \int_0^z \exp\left(\frac{-t^2}{2}\right) \mathrm{d}t \tag{15}$$

where Φ denotes the cumulative normal distribution function, P represents the probability and varies between 0 and 1, and z varies from $-\infty$ to $+\infty$ and can be calculated using Eq. (13).

3.4 Preparation of training dataset

We used the inventory map produced by Othman and Gloaguen (2013a). We classified the boundary of each landslide polygon into two zones: (1) the landslide depletion zone and (2) the landslide accumulation zone. The geometrical attributes are stored in a GIS database as a shape file and then rasterized the polygons by 15 m resolution. Only the depletion zones of the landslides are included in the susceptibility analysis (Atkinson and Massari, 1998; Van Den Eeckhaut et al., 2006; Thiery et al., 2007). Following literature suggestions (Bai et al., 2012; Xu et al., 2012; Erener and Duzgun, 2012), we sub-divided the landslides randomly into training and validation data subsets. The training dataset included 80 % of the pixels (11 137 pixels with landslides), which represent ~ 0.3 % of the total study area and the validation set included the remaining 20 % of the pixels.

We used this training dataset to calculate the LS for FR and WoE. However, the LR and PR models need a training dataset containing both pixels with landslides and pixels without landslides (Ozdemir and Altural, 2013; Ayalew and Yamagishi, 2005). Therefore, we randomly selected 11 137 pixels without landslides. Thus, the training dataset for the LR and PR models contain 11 137 pixels with landslides and 11 597 pixels without landslides. The predicted factors represent the independent variables while the class values (landslide-present and landslide-absent), i.e. 0 and 1 are the dependent variable. The pixels with information from the predictive factors were exported and saved as a text file. This file was analyzed using R software (Core Team: R, 2014) to obtain the estimation constants (α and β), which are important for calculating the probability (z).

3.5 Models uncertainty and models prediction skill

In order to recognize the best susceptibility model, we applied two prediction skill methods to the landslide validation datasets (20 % of the total landslide pixels). The first method is a quantitative measurement called the areas under the curve (AUC) of the Success Rate Curve (SRC). The AUC

is widely used to estimate the accuracy of LS models (Yesilnacar and Topal, 2005). A SRC is a two-dimensional plot. The x-axis is (100 - LS rank %) and the y-axis is cumulative percentage of validation landslide occurrence (%). An acceptable model should have an AUC of more than 50 % (Chung and Fabbri , 2003). The second prediction skill approach is the R index (Santacana et al., 2003; Baeza and Corominas, 2001; Schicker and Moon, 2012). It represents the ratio (%) between the area of landslides in an individual susceptibility class as a percentage of all landslides area and the area of an individual susceptibility class as a percentage area of all susceptibility classes. The R index is computed using Eq.(16).

$$R \text{ index} = \left(\frac{\left(\frac{L_i}{A_i}\right)}{\sum_1^n \left(\frac{L_i}{A_i}\right)} \right) \cdot 100 \tag{16}$$

where L_i is the area of landslides in susceptibility class i, $A_i =$ area occupied of susceptibility class i, and n is the number of susceptibility classes The LS values given by the four models were then classified software using natural breaks technique into five susceptibility classes : very high, high, moderate, low and safe (Ozdemir and Altural, 2013; Shahabi et al., 2014; Mărgărint et al., 2013; Intarawichian and Dasananda, 2011; Poli and Sterlacchini, 2007). We used the natural breaks method because it allows to gather similar values and to maximize the differences between classes. This characteristic makes the natural breaks useful when the LS histogram shows distinct breaks. (Mărgărint et al., 2013). The best model was determined as the model with highest AUC and R index values for “very high”, and “high” classes.

The uncertainty is one of the basic and important tests that provides a measure of the error associated with the susceptibility assessment approach (Guzzetti et al., 2006; Rossi et al., 2010). First, we tested the sensitivity of the susceptibility model to changes in the input data. Fifty landslide susceptibility maps were computed for each model using the same thematic information but with 50 different random selection for training datasets (80% of pixels with landslides), which called bootstrapping technique. For each of these fifty maps, AUC of the SRC was calculated using the validation datasets (20% of pixels with landslides). The sensitivity (variations of the AUC of the SRC) for each approach was estimated using a box plot diagram.

We then estimated the models error. 20,000 pixels were randomly selected and used for this purpose. For each model, we obtained descriptive statistics (including the mean and standard deviation) from the 50 estimated susceptibility maps using these selected pixels. The error plots show two standard deviations of these susceptibility estimates in the y-axis against their mean value in the x-axis (Guzzetti et al., 2006; Rossi et al., 2010).

4 Results

4.1 Predictive factors

Elevation in the study area ranges from 663 to 2360 m (Fig. 4a) with highest values in the East of the study area. More than 45 % of the landslides are located in the range of 900–1300 m, and 34 % of them are between 1500–1900 m. The TPI ranges from −258 to 406 m (Fig. 4b). Most landslides (70 %) are in the TPI range between −65–100 m. The slope aspect includes nine faces, which are flat, north, northeast, east, southeast, south, southwest, west, and northwest (Fig. 4a). 64 % of the landslides faced north to east direction. The maximum slope gradient is 65°. The results show that about 82 % of the landslides occur when the slope is between 10 to 35° (Fig. 4d; Table 1). The HI range between 0.1 and 0.7 (Fig. 4e), and 86.5 % of landslides occur in the range between 0.35 and 0.6 (V-shaped and entrenched valleys). Curvature ranges between −41.78 and 49.78 (Fig. 4f), plan curvature ranges between −25.79 and 26.48, and profile curvature ranges between −26.76 and 21.86 and there is no clear relation of landslide distribution and the type of curvatures. Since curvature, plan curvature and profile curvature have high correlation (more than 0.85) with each other, the only regular curvature was used as a prediction factor in the following analysis (Fig. 4f).

The study area consists of different lithostratigraphic units. Othman and Gloaguen (2014) have subdivided the Mawat area into eight lithological classes. These are (1) ultramafic, (2) gabbro, (3) metabasalt and basalt, (4) gabbro to diorite with ultramafic inclusions, (5) limestone, marble, calc-schist and clastics, (6) clastics, (7) conglomerate, and (8) floodplain and valley fill sediments (Fig. 5a). The limestone, metabasalt and clastic rocks make up of 83 % of the totaltotal landslides area. The farthest distance of the image discontinuities from the landslide in the study area is 2856 m (Fig. 5b). The area within the buffer zone of 450 m around image discontinuities covers about 68 % of so far published faults in the area (Fig. 5a; Al-Mehaidi, 1974. If the buffer is extended to 1000 m 96 % of landslides fall into this area (Fig. 5b).

The maximum TWI reaches 19 (Fig. 6a). The TWI value range between 6 and 9 comprises more than 54 % of all landslides. The NDVI ranges from −0.12 to 0.75. The majority of landslides (92 %) occur in non-vegetated areas with NDVI values smaller than 0.22 (Fig. 6b). Eight classes of land cover were derived in the study area. These are urban and built-up land, vegetated land, cultivated land, burn land, harvested land, igneous and/or metamorphic rocks, and sedimentary rocks. Most landslides occur in sedimentary and igneous rock classified land cover classes (Fig. 6c). The annual precipitation range is 763–896 mm. It increases from SE towards NW of the study area. The class < 833 mm comprises 45 % of all landslides, although the area of this class covers only 25 % of the total study area (Fig. 6d). The drainage density ranges from 0.58–2.64 and the farthest point in the map area from the drainage is 936 m (Fig. 6e). Areas with moderate drainage density correlate with landslide occurrence significantly higher than the areas with low and high drainage density.

The highest density of landslides has a distance from 300 to 400 m from the drainage network (Fig. 6f). We classified all above-mentioned factors to use them in FR and WoE models (Table 1).

4.2 Landslide susceptibility assessment

The LS maps have been prepared using four different models. We evaluated the predictive factors qualitatively to select influencing factors and to enhance the prediction accuracy of the LS map.

4.2.1 Landslide susceptibility assessment using frequency ratio and weight of evidence

The relationships between landslides and landslide prediction factors using FR and WoE models are shown in Table 1. The precipitation class $< 833\,\mathrm{mm}$ yields the highest value for FR of 1.82 and a C weight of 0.911 (Table 1). In the lithological classes, gabbro to diorite yields the highest FR value (1.82) and a C of 0.795 while the clastic rocks class yields a FR of 1.799, and a C of 0.617. The harvested land class yields a FR value equal to 1.353 and a C weight of 0.340, indicating a high probability of landslide occurrence. The highest FR value (2.118) and a C weight of 0.869 are obtained for elevations between 1701 and 1900 m. The slope class between 15 and 20° yields highest FR values (1.399) and a C weight of 0.426. The distance from lineaments between 750 and $1000\,\mathrm{m}$ is associated to the highest probability of landslide occurrence with values for FR of 1.287 and a C weight of 0.285. Areas located 300 to 400 m (FR=1.322 and C weight=0.313), and areas with a drainage-density between 1.25 and 1.55 (FR=1.534 and C weight=0.522) are most sensible to landslides.

In the case of aspect, most landslides occurred facing northeast and east where the weight of FE is > 2, and the weight of C is > 0.86. In the case of the hypsometric integral, the class between 0.35 and 0.425 yields highest FR and C weights with values of 1.705 and 0.769, respectively. For TWI, the highest landslide probability was determined for the TWI class > 10 with values for FR of 1.205 and 0.214 for the C weight. Highest FR and C weight values of 1.123 and 0.152, respectively, were obtained for the TPI < -65. Decreasing NDVI values inversely correlate with FR values in the study area except for the lowest class. The 0.12–0.15 class has the highest FR weight of 1.268 while the C weight is 0.333 (Table 1).

We tested more than 10 different combinations of prediction factors in order to select the best individual combination for the FR and WoE models. The final LS maps based on the FR and WoE models were calculated based on a total of 12 factors. The ranges of the prediction factor estimation weights are the difference in estimation weight between the largest and smallest values of each prediction factor, which can be calculated by applying the prediction model equations Eqs. (5, 7, 12, and 14). These ranges are good indicator of the sensitivity of a factor to landslide occurrences (i.e. the prediction factor, which displays a wide range is more sensitive to the occurrence of landslides than a factor with a narrow range. Figure 7a shows that lithology, slope aspect and elevation are more

sensitive than other factors in the FR models, while the WoE model is more sensitive to lithology, hypsometric integral and slope aspect factors. Curvature and land cover are not considered because they decreased the model performance by decreasing the AUC of the SRC. The LS map has been classified by equal areas and grouped into five classes with frequency levels of 20, 40, 60, and 80 %. These are very high, high, moderate, low and safe susceptibility zones, respectively. The best distributions of the LS of FR and WoE are shown in Figs. 8a and 6b, respectively. The FR and WoE LS maps show that the spatial distribution are a bit similar, where 65 % of "very high" and "high" susceptibility classes are shared between these two models.

4.2.2 Landslide susceptibility assessment using logistic and probit regressions

1.2 % of the study area (22 734 training pixel) was used to derive the coefficients of PR and LR. The model-building process for both LR and PR started with 16 prediction factors. The landslide prediction factors considered in this study are shown in Table 1. In the last processing step, nine factors were interpreted as non-significant (p-value > 0.05) and therefore excluded from the analysis. We used the seven remaining factors (namely HI, slope, TWI, NDVI, precipitation, lithology and aspect), which were significant (p-value < 0.05; Table 2).

In both the probit and logistic regression the lithology, the slope aspect and the NDVI appear as the major factors controlling the landslides occurrences (Fig. 7b).

The factors with an odd ratio of more than 1 are positively related to the occurrence of landslides and the factors with an odd ratio of less than 1 are negatively related to the landslide occurrence. Those factors with an odd ratio of 1, like precipitation and slope gradient factors are neutral to the occurrence of landslides in the study area. Obtained odd ratios (Table 2), for slope gradient and precipitation is 1; those for the hypsometric integral, TWI, the clastic and limestone lithological classes, and the N, NE, E, SE and NW aspect directions are more than 1. Others are less than 1. In particular, the factor "NE aspect" has the strongest effect on the development of landslides than any other parameter, where the odd ratio of the probit and the logistic regressions are 3.95 and 2.33, respectively. The best susceptibility zonations obtained using LR and PR are shown in Figs. 8c and 6d, respectively. The PR and the LR LS maps show a similar spatial distribution, where 99.7 % of "very high" and "high" susceptibility classes are shared between these two models.

5 Discussion

GIS-based techniques are a powerful and important tool to assess and map landslide susceptibility. In previous studies, FR, LR, and WoE methods were used either separately (e.g. Shahabi et al., 2014; Wang et al., 2013; Pradhan and Lee, 2010; Das et al., 2012), or compared with other susceptibility models (e.g. Ozdemir and Altural, 2013). In this study, we compared the three above-mentioned models to the PR model, which has never been applied for LS mapping before. Each model shows

advantages and disadvantages. FR and WOE models prove themselves to be rather simple and easy to apply. In contrast, LR and PR models appear more complex as the result of the data conversion from GIS standard formats to the format required by the statistical software (Park et al., 2013). The FR and WoE methods allow the evaluation of relationships between a dependent (landslides) and several independent variables (predicting factors) only in a discrete form. On the other hand, LR and PR allow to evaluate the continuous independent variables in addition to discrete forms (Shahabi et al., 2014; Wang et al., 2013; Schicker and Moon, 2012).

The four LS maps show a similar spatial distribution. The PR and LR models gave almost the same results. In some areas, the FR and WoE models show significant variations with respect to PR and LR. This is mainly the case in the southern and western parts of the study area (Fig. 8). Only 25 % of the very high susceptibility class is shared among all models.

In order to verify the results of the four LS models, we made a comparison between them using AUC and R index. AUCs of the of SRC plot suggest a similar efficiency for the LS maps obtained from the PR, LR and WoE models with values of 81.86, 81.83 and 81.61 %, respectively. Only the FR-based LS map obtained a significantly lower AUC of 78.31 % (Fig. 9a). The PR and LR models show almost identical SRC curves (Fig. 9a). R index values for the final WoE map indicate that the sum of "very high" and "high" landslides susceptibility classes contains 89.42 % of the validation landslide areas, while in the final PR, LR, and FR maps it contains 86.29, 86.22, and 84.22 % of the validation landslide areas, respectively (Fig. 9b). All other zones include validation landslide areas < 16 %. The safe susceptibility class of the final WoE map contains 0.75 % of the validation landslide areas (less than the final PR, LR, and FR maps). Accounting for both prediction skills results (i.e. AUC and R index), WoE can be assumed as the best method used in this paper followed by PR, LR and FR. The differences between the AUC for PR, LR and WoE models are < 0.35 %, while for the R index they reach 5 % for the "very high" susceptibility class, and 3.2 % for the "very high" and "high" classes. The PR, LR, and WoE models are comparatively good estimators for the LS. Our results indicate that the LR model is better than the FR model. This is consistent with previous studies (Shahabi et al., 2014; Choi et al., 2012; Park et al., 2013; Yilmaz, 2009; Lee et al., 2012). The results of this paper also agree with Suh et al. (2011) who reported that the WoE model is better than the FR model. Indeed, the AUC of the WoE model is ~ 3.55 % higher than the AUC of the FR model.

Figures 10 and 11 show measures of the uncertainty for the four LS models. The FR approach shows lesser error than all other approaches, where the 2 standard deviations of the obtained probability estimate are less than 0.05. In all models, the measure of 2 standard deviations of the obtained probability estimate are lower than 0.15. The FR and WoE error plots show a similar (Fig. 10a and b). The error is lesser in FR than WoE. In both approaches the values of the 2 standard deviations are distributed along "bands" as a result of the discrete modelization. Some classes, especially those that have a wide range in a small area give the highest 2 standard deviations. The banding'bands'

distribution is more clear pronounced in the WoE approach because this model uses a logarithmic scale. The PR and LR give some banding as well because of that the input predictive parameters have discrete form. PR has less error than LR, but both approaches show similar behaviors. Highest 2 standard deviations are found for the intermediate values of the probability. According toGuzzetti et al. (2006), the obtained estimate of the intermediate values is highly variable, and, therefore, unreliable (Fig. 10c and d).

Figure 11 shows the sensitivity of our models to input data. For each model, the boxplot represents the distribution of the area under the success rate curve obtained from 50 different datasets. The PR method appears to be more sensitive to the input dataset than the other methods (Fig. 11). Taking into account models uncertainties, the WoE appears to be the best method followed by the PR and LR methods. The performance of the FR method is slightly lower than the others (Fig. 11).

Previous works which applied generalized linear models have only focused on LR. The PR has never been used before for LS mapping although many popular statistical software such as SPSS and R include this function. The sensitivity median of the PR models is slightly better than the sensitivity median of the LR model ($\sim 0.02\%$; Fig. 11). The PR model yields range of the sensitivity wider than the LR model, which sometimes gives slightly better results than the LR model. This supports the finding of Bottai et al. (2010). Our results indicate that the PR model is a valuable approach. The different datasets of factor groups we tested show that the AUCs of the PR model are $\pm 1\,\%$ than the AUC of the LR model (Fig. 11). The "high" and "very high" classes of the R index for the PR model are also slightly higher compared to the LR model (Fig. 9b).

The selection of the predicting factors plays a dominant role to increase the AUC of the LS map (Carrara et al., 1995; Capitani et al., 2013a; Van Den Eeckhaut et al., 2006). Careful consideration of all relevant factors is required to adequately assess the weightings of factors according to specific site conditions, especially for FR and WoE. It should be noted that the number and boundary of classes can strongly influence the obtained results of the FR and WoE methods. The estimation range of all four models (Fig. 7) indicates that lithology and slope aspects played major roles in frequent landslide occurrences in the Mawat area. All models show that lithology is more effective than another factor. This is likely due to the variance in the cohesion and permeability of the rock types (Ozdemir and Altural, 2013; Garcia-Rodriguez et al., 2008; Dai et al., 2001). In addition, the slope aspect has a significant impact on landsliding because it controls the exposure to sunlight, winds, rainfall (Yalcin et al., 2011), and vegetation cover (Garcia-Rodriguez et al., 2008).

Both the curvature and the HI are affected by the slope shape of major, medium and small landslides. However, the use of HI as prediction factor instead of the curvature increased the AUC of our LS maps by $\sim 2\,\%$. This significant increase is related to the sensitivity of the HI values to erosional processes (Perez-Pena et al., 2009). The HI coefficients show that areas with V-shaped valleys or entrenched rivers are more affected by landsliding than other types of landforms. The increase in landslides frequency is also related to the decrease of NDVI value (i.e. a lack of appropriate

vegetation cover). The landslides frequency is decreasing with increasing precipitation where the precipitation increases $\sim 131\,\mathrm{mm\,yr^{-1}}$ to the N-NW seem to decrease the landslides frequency. It is known that the role of precipitation as significant factor to explain landslides is strongly affected by the landscape dynamics and geology (Yalcin et al., 2011). High to moderate slope areas are more risky than low slope areas, independently of precipitation amounts. The same applies for the increased risk in areas with soft rocks compared to tough rocks. Therefore, it seems that the influence of other factors such as lithology and morphological dynamics such as slope aspect and HI is greater compared to the variation of the precipitation.

Combining the TPI with the other significant prediction factors also increased the AUC of FR and WoE by $\sim 1\,\%$. Distance to lineaments (created with TecLines, Rahnama and Gloaguen, 2014a, b) contributed to improve the AUC of the WoE and FR methods by $\sim 2\,\%$. The TPI and distance to lineaments did not improve significantly the LS maps obtained from the LR and PR models. However, Rahnama et al. (2015) reported that including the distance to lineaments significantly improves the detection of landslide occurrences in the northeast of Afghanistan not only in FR and WoE but in LR methods as well.

6 Conclusions

For the first time, PR was applied together with FR, WoE and LR to compute landslides susceptibility maps for the Mawat area, Kurdistan Region, NE Iraq. These four methods have not been compared before and we thus attempted to determine their accuracy in landslide susceptibility mapping. We utilized 16 prediction factors, most of which were derived from VNIR ASTER satellite data. Two of them (i.e. lithology and slope aspect) have more influence than other factors in landslide occurrences. This study also uses TPI as prediction factor in order to increase the estimation accuracy of the LS. This paper demonstrates that the hypsometric integral yields better results than slope curvatures, and increases the area under the curve by $\sim 2\,\%$. The distance-to-lineaments map contributed to an increase of the area under the curve for the FR and WoE landslide susceptibility maps by $\sim 2\,\%$. This study suggests that the PR and LR models have a similar behavior, while the WoE and FR models are close of each other. Processing steps of the FR and WoE models are relatively simple and easy compared to the PR and LR, which need a preliminary conversion of data. Obtained results in this study indicate that the PR, LR, and WoE models are good estimators of the LS. The WoE model has the overall highest prediction accuracy. The PR method, which we applied here for the first time to map LS, proved itself to be a viable alternative to other methods. It even outperformed the LR model in terms of prediction skills (i.e., AUC and R Index), but it is more dependent to the used dataset combinations. The error and the variability associated with the frequency ratio model are less than other landslide susceptibility models.

Author contributions. Arsalan Ahmed Othman prepared and processed the data and accomplished the study. He wrote the manuscript. Richard Gloaguen outlined the research and supported the analysis and discussion. He also supervised the writing of the manuscript at all stages. Louis Andreani and Mehdi Rahnama assisted with the extraction of lineaments and geomorphic indices. All authors checked and revised the manuscript.

Acknowledgements. The research was supported by the Ministry of Higher Education and Scientific Research of Iraq (MoHESR), and by the German Academic Exchange Service (DAAD). We are grateful to the Geological Survey of Iraq for providing the data and supporting the fieldwork.

References

Abrams, M. and Hook, S.: ASTER user handbook (Version 2), Report, California Institute of Technology, Pasadena, USA, 2001.

Agard, P., Omrani, J., Jolivet, L., Whitechurch, H., Vrielynck, B., Spakman, W., Monié, P., Meyer, B., and Wortel, R.: Zagros orogeny: a subduction-dominated process, Geol. Mag., 148, 692–725, doi:10.1017/S001675681100046X, 2011.

Akgun, A.: A comparison of landslide susceptibility maps produced by logistic regression, multi-criteria decision, and likelihood ratio methods: a case study at İzmir, Turkey, Landslides, 9, 93–106, doi:10.1007/s10346-011-0283-7, 2012.

Al-Mehaidi, H. M.: Geological investigation of Mawat-Chuwarta area, northeastern Iraq, Report 609, GEOSURV, Baghdad, Iraq, 1974.

Al-Rubaiay, A. T. and Al-Dulaimi, T. Y.: Series of land use land cover maps of Iraq scale 1 : 250 000, Sulaimaniya quadrangle sheet NI-38-3 (LULCM 10), Report, GEOSURV, Baghdad, Iraq, 2012.

Alavi, M.: Tectonics of Zagros Oroginic Belt of Iran: new data and interpretations, Tectonophysics, 229, 221–238, 1994.

Alavi, M.: Regional stratigraphy of the Zagros Fold – thrust belt of Iran and its proforeland evolution, Am. J. Sci., 304, 1–20, 2004.

Aldrich, J. and Nelson, F.: Linear Probability, Logit, and Probit Models, SAGE Publications, available at: http://books.google.de/books?id=z0tmctgE1OYC (last access: 17 January 2015), 1984.

Althuwaynee, O. F., Pradhan, B., Park, H.-J., and Lee, J. H.: A novel ensemble bivariate statistical evidential belief function with knowledge-based analytical hierarchy process and multivariate statistical logistic regression for landslide susceptibility mapping, Catena, 114, 21–36, doi:10.1016/j.catena.2013.10.011, 2014.

Atkinson, P. M. and Massari, R.: Generalised linear modelling of susceptibility to landsliding in the central Apennines, Italy, Comput. Geosci., 24, 373–385, 1998.

Ayalew, L. and Yamagishi, H.: The application of GIS-based logistic regression for landslide susceptibility mapping in the Kakuda-Yahiko Mountains, Central Japan, Geomorphology, 65, 15–31, doi:10.1016/j.geomorph.2004.06.010, 2005.

Ayalew, L., Yamagishi, H., Marui, H., and Kanno, T.: Landslides in Sado Island of Japan: Part II, GIS-based susceptibility mapping with comparisons of results from two methods and verifications, Eng. Geol., 81, 432–445, doi:10.1016/j.enggeo.2005.08.004, 2005.

Baeza, C. and Corominas, J.: Assessment of shallow landslide susceptibility by means of multivariate statistical techniques, Earth Surf. Proc. Land., 26, 1251–1263, 2001.

Bai, S., Wang, J., Zhang, Z., and Cheng, C.: Combined landslide susceptibility mapping after Wenchuan earthquake at the Zhouqu segment in the Bailongjiang Basin, China, Catena, 99, 18–25, doi:10.1016/j.catena.2012.06.012, 2012.

Beven, K. J. and Kirkby, M. J.: A physically based, variable contributing area model of basin hydrology/Un modelle a base physique de zone d'appel variable de l'hydrologie du bassin versant, Hydrol. Sci. Bull., 24, 43–69, doi:10.1080/02626667909491834, 1979.

Bottai, M., Cai, B., and McKeown, R. E.: Logistic quantile regression for bounded outcomes, Stat. Med., 29, 309–317, 2010.

Buday, T. and Suk, M.: Report on the geological survay in NE Iraq between Halabja and Qala'a Diza, Report, GEOSURV, Baghdad, Iraq, 1978.

Calo, F., Ardizzone, F., Castaldo, R., Lollino, P., Tizzani, P., Guzzetti, F., Lanari, R., Angeli, M.-G., Pontoni, F., and Manunta, M.: Enhanced landslide investigations through advanced DInSAR techniques: the Ivancich case study, Assisi, Italy, Remote Sens. Environ., 142, 69–82, doi:10.1016/j.rse.2013.11.003, 2014.

Capitani, M., Ribolini, A., and Bini, M.: The slope aspect: a predisposing factor for landsliding?, CR Geosci., 345, 427–438, doi:10.1016/j.crte.2013.11.002, 2013a.

Capitani, M., Ribolini, A., and Federici, P. R.: Influence of deep-seated gravitational slope deformations on landslide distributions: a statistical approach, Geomorphology, 201, 127–134, 2013b.

Carrara, A., Cardinali, M., Guzzetti, F., and Reichenbach, P.: GIS technology in mapping landslide hazard, in: Geographical Information Systems in Assessing Natural Hazards, vol. 5 of Advances in Natural and Technological Hazards Research, book section 8, Springer Netherlands, 135–175, doi:10.1007/978-94-015-8404-3_8, 1995.

Chen, W., Li, X., Wang, Y., and Liu, S.: Landslide susceptibility mapping using LiDAR and DMC data: a case study in the Three Gorges area, China, Environ. Earth Sci., 70, 673–685, 2013.

Choi, J., Oh, H.-J., Lee, H.-J., Lee, C., and Lee, S.: Combining landslide susceptibility maps obtained from frequency ratio, logistic regression, and artificial neural network models using ASTER images and GIS, Eng. Geol., 124, 12–23, doi:10.1016/j.enggeo.2011.09.011, 2012.

CHRR, CIESIN, and NGI: Global Landslide Hazard Distribution, available at: http://sedac.ciesin.columbia.edu/data/set/ndh-landslide-hazard-distribution (last acces: 17 January 2015), 2005.

Core Team: R: a Language and Environment for Statistical Computing. R Foundation for Statistical Computing, Vienna, Austria, http://www.Rproject.org, 2014.

Conforti, M., Pascale, S., Robustelli, G., and Sdao, F.: Evaluation of prediction capability of the artificial neural networks for mapping landslide susceptibility in the Turbolo River catchment (northern Calabria, Italy), Catena, 113, 236–250, doi:10.1016/j.catena.2013.08.006, 2014.

Corsini, A., Cervi, F., and Ronchetti, F.: Weight of evidence and artificial neural networks for potential groundwater spring mapping: an application to the Mt. Modino area (Northern Apennines, Italy), Geomorphology, 111, 79–87, doi:10.1016/j.geomorph.2008.03.015, 2009.

Costanzo, D., Rotigliano, E., Irigaray, C., Jimenez-Peralvarez, J. D., Chacon, J.: Factors selection in landslide susceptibility modelling on large scale following the gis matrix method: application to the river Beiro basin (Spain), Nat. Hazards Earth Syst. Sci., 12, 327–340, doi:10.5194/nhess-12-327-2012, 2012.

Chung, C. and Fabbri, A.: Validation of Spatial Prediction Models for Landslide Hazard Mapping. Natural Hazards, 30, 451–472, doi:10.1023/B%3ANHAZ.0000007172.62651.2b, 2003.

Dai, F. C., Lee, C. F., Li, J., and Xu, Z. W.: Assessment of landslide susceptibility on the natural terrain of Lantau Island, Hong Kong, Environ. Geol., 40, 381–391, doi:10.1007/s002540000163, 2001.

Das, I., Stein, A., Kerle, N., and Dadhwal, V. K.: Landslide susceptibility mapping along road corridors in the Indian Himalayas using Bayesian logistic regression models, Geomorphology, 179, 116–125, doi:10.1016/j.geomorph.2012.08.004, 2012.

De Reu, J., Bourgeois, J., Bats, M., Zwertvaegher, A., Gelorini, V., De Smedt, P., Chu, W., Antrop, M., De Maeyer, P., Finke, P., Van Meirvenne, M., Verniers, J., and Crombe, P.: Application of the topographic position index to heterogeneous landscapes, Geomorphology, 186, 39–49, 2013.

DigitalGlobe: QuickBird Imagery Products – Product Guid, Report, Global Land Cover Facility, Longmont, Colorado, USA, 2006.

Ercanoglu, M.: Landslide susceptibility assessment of SE Bartin (West Black Sea region, Turkey) by artificial neural networks, Nat. Hazards Earth Syst. Sci., 5, 979–992, doi:10.5194/nhess-5-979-2005, 2005.

Erener, A. and Duzgun, H. S. B.: Landslide susceptibility assessment: what are the effects of mapping unit and mapping method?, Environ. Earth Sci., 66, 859–877, 2012.

ESRI: ArcGIS Desktop: Release 10, USA, 2011.

ESRI: ArcGIS help library, Report, Environmental Systems Research Institute, USA, 2012.

Fouad, S. F.: Tectonic map of Iraq, scale 1 : 1,000,000, GEOSURV, Baghdad, Iraq, 2010.

García-Rodríguez, M. J. and Malpica, J. A.: Assessment of earthquake-triggered landslide susceptibility in El Salvador based on an Artificial Neural Network model, Nat. Hazards Earth Syst. Sci., 10, 1307–1315, doi:10.5194/nhess-10-1307-2010, 2010.

Garcia-Rodriguez, M. J., Malpica, J. A., Benito, B., and Diaz, M.: Susceptibility assessment of earthquake-triggered landslides in El Salvador using logistic regression, Geomorphology, 95, 172–191, 2008.

Guzzetti, F.: Landslide hazard and risk assessment, dissertation, Bonn University, Bonn, 2006.

Guzzetti, F., Carrara, A., Cardinali, M., and Reichenbach, P.: Landslide hazard evaluation: a review of current techniques and their application in a multi-scale study, Central Italy, Geomorphology, 31, 181–216, doi:10.1016/S0169-555X(99)00078-1, 1999.

Guzzetti, F., Cardinali, M., Reichenbach, P., and Carrara, A.: Comparing landslide maps: a case study in the Upper Tiber River Basin, Central Italy, Environ. Manage., 25, 247–263, doi:10.1007/s002679910020, 2000.

Guzzetti, F., Reichenbach, P., Cardinali, M., Galli, M., and Ardizzone, F.: Probabilistic landslide hazard assessment at the basin scale, Geomorphology, 72, 272–299, 2005.

Guzzetti, F., Reichenbach, P., Ardizzone, F., Cardinali, M., and Galli, M.: Estimating the quality of landslide susceptibility models, Geomorphology, 81, 166–184, 2006.

Intarawichian, N. and Dasananda, S.: Frequency ratio model based landslide susceptibility mapping in lower Mae Chaem watershed, Northern Thailand, Environ. Earth Sci., 64, 2271–2285, doi:10.1007/s12665-011-1055-3, 2011.

Jassim, S. Z. and Goff, J. C.: Geology of Iraq, Dolin, Brno, Czech Republic, 2006.

Kayastha, P., Dhital, M. R., and De Smedt, F.: Application of the analytical hierarchy process (AHP) for landslide susceptibility mapping: a case study from the Tinau watershed, west Nepal, Comput. Geosci., 52, 398–408, doi:10.1016/j.cageo.2012.11.003, 2013.

Kleinbaum, D. and Klein, M.: Survival Analysis: a Self-Learning Text, 3rd Edn., Springer, available at: http://books.google.de/books?id=v3FZngEACAAJ (last access: 13 January 2015), 2011.

Lawa, F. A., Koyi, H., and Ibrahim, A.: Tectono-stratigraphic evolution of the NW segment of the Zagros fold-thrust belt, Kurdistan, NE Iraq, J. Petrol. Geol., 36, 75–96, 2013.

Lee, M. J., Choi, J. W., Oh, H. J., Won, J. S., Park, I., and Lee, S.: Ensemble-based landslide susceptibility maps in Jinbu area, Korea, Environ. Earth Sci., 67, 23–37, a 2012.

Lee, S.: Landslide detection and susceptibility mapping in the Sagimakri area, Korea using KOMPSAT-1 and weight of evidence technique, Environ. Earth Sci., 70, 3197–3215, 2013.

Lee, S. and Min, K.: Statistical analysis of landslide susceptibility at Yongin, Korea, Environ. Geol., 40, 1095–1113, doi:10.1007/s002540100310, 2001.

Lee, S. and Talib, J. A.: Probabilistic landslide susceptibility and factor effect analysis, Environ. Geol., 47, 982–990, 2005.

Lee, S., Ryu, J., Min, K., and Won, J.: Development of two artificial neural network methods for landslide susceptibility analysis, in: Geoscience and Remote Sensing Symposium, 2001, IGARSS '01, IEEE 2001 International, vol. 5, 9–13 July 2001, Sydney, NSW, 2364–2366, 2001.

Lee, S., Choi, J., Chwae, U., and Chang, B.: Landslide susceptibility analysis using weight of evidence, vol. 5, 2865–2867, available at: http://www.scopus.com/inward/record.url?eid=2-s2.0-0036398928&partnerID=40&md5=dae165d8fbccd72155aae1371bfe966d (last access: 13 January 2015), 2002a.

Lee, S., Choi, J., and Min, K.: Landslide susceptibility analysis and verification using the Bayesian probability model, Environ. Geol., 43, 120–131, doi:10.1007/s00254-002-0616-x, 2002b.

Lepore, C., Kamal, S. A., Shanahan, P., and Bras, R. L.: Rainfall-induced landslide susceptibility zonation of Puerto Rico, Environ. Earth Sci., 66, 1667–1681, 2012.

Lin, L. L., Wang, C. W., Chiu, C. L., and Ko, Y. C.: A study of rationality of slopeland use in view of land preservation, Paddy Water Environ., 9, 257–266, 2011.

Ma'ala, K.: The geology of Sulaimaniya Quadrangle sheet no. NI-38-3, Scale 1 : 25 0000, Report, GEOSURV, Baghdad, Iraq, 2008.

Mancini, F., Ceppi, C., and Ritrovato, G.: GIS and statistical analysis for landslide susceptibility mapping in the Daunia area, Italy, Nat. Hazards Earth Syst. Sci., 10, 1851–1864, doi:10.5194/nhess-10-1851-2010, 2010.

Mantovani, F., Soeters, R., and Van Westen, C. J.: Remote sensing techniques for landslide studies and hazard zonation in Europe, Geomorphology, 15, 213–225, doi:10.1016/0169-555X(95)00071-C, 1996.

McCullagh, P. and Nelder, J.: Generalized Linear Models, Routledge, Chapman & Hall, Incorporated, available at: http://books.google.de/books?id=_ku8QgAACAAJ (last access: 13 January 2015), 1983.

Metternicht, G., Hurni, L., and Gogu, R.: Remote sensing of landslides: an analysis of the potential contribution to geo-spatial systems for hazard assessment in mountainous environments, Remote Sens. Environ., 98, 284–303, doi:10.1016/j.rse.2005.08.004, 2005.

Meyer, N. K., Schwanghart, W., Korup, O., Romstad, B. A., and Etzelmüller, B.: Estimating the topographic predictability of debris flows, Geomorphology, 207, 114–125, doi:10.1016/j.geomorph.2013.10.030, 2014.

Mohammady, M., Pourghasemi, H. R., and Pradhan, B.: Landslide susceptibility mapping at Golestan Province, Iran: a comparison between frequency ratio, Dempster-Shafer, and weights-of-evidence models, J. Asian Earth Sci., 61, 221–236, doi:10.1016/j.jseaes.2012.10.005,2012.

Moore, I. D., Grayson, R. B., and Ladson, A. R.: Digital terrain modelling: a review of hydrological, geomorphological, and biological applications, Hydrol. Process., 5, 3–30, 1991.

Mărgărint, M. C., Grozavu, A., and Patriche, C. V.: Assessing the spatial variability of coefficients of landslide predictors in different regions of Romania using logistic regression, Nat. Hazards Earth Syst. Sci., 13, 3339–3355, doi:10.5194/nhess-13-3339-2013, 2013.

Nefeslioglu, H. A., Duman, T. Y., and Durmaz, S.: Landslide susceptibility mapping for a part of tectonic Kelkit Valley (Eastern Black Sea region of Turkey), Geomorphology, 94, 401–418, 2008a.

Nefeslioglu, H. A., Gokceoglu, C., and Sonmez, H.: An assessment on the use of logistic regression and artificial neural networks with different sampling strategies for the preparation of landslide susceptibility maps, Eng. Geol., 97, 171–191, 2008b.

Othman, A. and Gloaguen, R.: Automatic extraction and size distribution of landslides in Kurdistan Region, NE Iraq, Remote Sensing, 5, 2389–2410, doi:10.3390/rs5052389, 2013a.

Othman, A. and Gloaguen, R.: River courses affected by landslides and implications for hazard assessment: a high resolution remote sensing case study in NE Iraq–W Iran, Remote Sensing, 5, 1024–1044, doi:10.3390/rs5031024 2013b.

Othman, A. and Gloaguen, R.: Improving lithological mapping by SVM classification of spectral and morphological features: the discovery of a new chromite body in the Mawat Ophiolite Complex (Kurdistan, NE Iraq), Remote Sensing, 6, 6867–6896, doi:10.3390/rs6086867, 2014

Ozdemir, A. and Altural, T.: A comparative study of frequency ratio, weights of evidence and logistic regression methods for landslide susceptibility mapping: Sultan Mountains, SW Turkey, J. Asian Earth Sci., 64, 180–197, doi:10.1016/j.jseaes.2012.12.014, 2013.

Park, S., Choi, C., Kim, B., and Kim, J.: Landslide susceptibility mapping using frequency ratio, analytic hierarchy process, logistic regression, and artificial neural network methods at the Inje area, Korea, Environ. Earth Sci., 68, 1443–1464, doi:10.1007/s12665-012-1842-5, 2013.

Peng, L., Niu, R., Huang, B., Wu, X., Zhao, Y., and Ye, R.: Landslide susceptibility mapping based on rough set theory and support vector machines: a case of the Three Gorges area, China, Geomorphology, 204, 287–301, doi:10.1016/j.geomorph.2013.08.013, 2014.

Perez-Pena, J., Azanon, J., and Azor, A.: CalHypso: an ArcGIS extension to calculate hypsometric curves and their statistical moments. Applications to drainage basin analysis in {SE} Spain, Comput. Geosci., 35, 1214–1223, doi:10.1016/j.cageo.2008.06.006, 2009.

Petley, D.: Global patterns of loss of life from landslides, Geology, 40, 927–930, 2012.

Pike, R. J. and Wilson, S. E.: Elevation-relief ratio, hypsometric integral, and geomorphic area-altitude analysis, Bull. Geol. Soc. Am., 82, 1079–1084, 1971.

Poli, S. and Sterlacchini, S.: Landslide representation strategies in susceptibility studies using weights-of-evidence modeling technique, Nat. Resour. Res., 16, 121–134, 2007.

Pradhan, B. and Lee, S.: Landslide susceptibility assessment and factor effect analysis: backpropagation artificial neural networks and their comparison with frequency ratio and bivariate logistic regression modelling, Environ. Model. Softw., 25, 747–759, doi:10.1016/j.envsoft.2009.10.016, 2010.

Pradhan, B., Singh, R. P., and Buchroithner, M. F.: Estimation of stress and its use in evaluation of landslide prone regions using remote sensing data, Adv. Space Res., 37, 698–709, 2006.

Qiao, G., Lu, P., Scaioni, M., Xu, S., Tong, X., Feng, T., Wu, H., Chen, W., Tian, Y., Wang, W., and Li, R.: Landslide investigation with remote sensing and sensor network: from susceptibility mapping and scaled-down simulation towards in situ sensor network design, Remote Sensing, 5, 4319–4346, 2013.

Rahnama, M. and Gloaguen, R.: TecLines: a MATLAB-based toolbox for tectonic lineament analysis from satellite images and DEMs, Part 2: Line segments linking and merging, Remote Sensing, 6, 11468–11493, doi:10.3390/rs61111468, 2014a.

Rahnama, M. and Gloaguen, R.: TecLines: a MATLAB-based toolbox for tectonic lineament analysis from satellite images and DEMs, Part 1: Line segment detection and extraction, Remote Sensing, 6, 5938–5958, doi:10.3390/rs6075938, 2014b.

Rahnama, M., Gloaguen, R., and Othman, A.: The Effect of Lineaments on the Accuracy of Landslide Susceptibility Mapping: a Case Study in Part of Badakhshan Province, Afghanistan, TU Freiberg, Freiberg, Germany, 2015.

Regmi, N. R., Giardino, J. R., and Vitek, J. D.: Assessing susceptibility to landslides: using models to understand observed changes in slopes, Geomorphology, 122, 25–38, 2010.

Rossi, M., Guzzetti, F., Reichenbach, P., Mondini, A., and Peruccacci, S.: Optimal landslide susceptibility zonation based on multiple forecasts, Geomorphology, 114, 129–142, 2010.

Rouse, J., Haas, R., Schelle, J., Deering, D., and Harlan, J.: Monitoring the vernal advancement or retrogradation of natural vegetation, Report, NASA, College Station, Texas, 1974.

Santacana, N. A., Baeza, B., Corominas, J., De Paz, A., and Marturiá, J.: A GIS-based multivariate statistical analysis for shallow landslide susceptibility mapping in La Pobla de Lillet Area (Eastern Pyrenees, Spain), Nat. Hazards, 30, 281–295, doi:10.1023/B:NHAZ.0000007169.28860.80, 2003.

Scaioni, M., Longoni, L., Melillo, V., and Papini, M.: Remote sensing for landslide investigations an overview of recent achievements and perspectives, Remote Sensing, 6, 9600–9652, doi:10.3390/rs6109600, 2014.

Schicker, R. and Moon, V.: Comparison of bivariate and multivariate statistical approaches in landslide susceptibility mapping at a regional scale, Geomorphology, 161–162, 40–57, doi:10.1016/j.geomorph.2012.03.036, 2012.

Shahabi, H., Khezri, S., Ahmad, B. B., and Hashim, M.: Landslide susceptibility mapping at central Zab basin, Iran: a comparison between analytical hierarchy process, frequency ratio and logistic regression models, Catena, 115, 55–70, doi:10.1016/j.catena.2013.11.014, 2014.

Shahzad, F. and Gloaguen, R.: TecDEM: a MATLAB based toolbox for tectonic geomorphology, Part 2: Surface dynamics and basin analysis, Comput. Geosci., 37, 261–271, doi:10.1016/j.cageo.2010.06.009, 2011.

Sissakian, V. K.: Geological evolution of the Iraqi Mesopotamia Foredeep, inner platform and near surroundings of the Arabian Plate, J. Asian Earth Sci., 31, 152–163, doi:10.1016/j.jseaes.2012.09.032, 2012.

Sissakian, V. K., Ahad, I. A., and Qambar, A.: Series of geological hazards map of Iraq sulimanyah quadrangle, scale 1 : 250 000, sheet No. NI-38-3, Report, GEOSURV, Baghdad, Iraq, 2004.

Smirnov, V. and Nelidov, V.: Report on 1 : 200,000 prospecting-correlation of the Sulimaniya-Choarta-Penjwin area carried out in 1961, Report, GEOSURV, Baghdad, Iraq, 1962.

Strahler, A. N.: Hypsometric (area-altitude) analysis of erosional topography, Geol. Soc. Am. Bull., 63, 1117–1142, 1952.

Suh, J., Choi, Y., Roh, T.-D., Lee, H.-J., and Park, H.-D.: National-scale assessment of landslide susceptibility to rank the vulnerability to failure of rock-cut slopes along expressways in Korea, Environ. Earth Sci., 63, 619–632, doi:10.1007/s12665-010-0729-6, 2011.

Thiery, Y., Malet, J. P., Sterlacchini, S., Puissant, A., and Maquaire, O.: Landslide susceptibility assessment by bivariate methods at large scales: application to a complex mountainous environment, Geomorphology, 92, 38–59, 2007.

Tseng, C. M., Lin, C. W., and Hsieh, W. D.: Landslide susceptibility analysis by means of event-based multi-temporal landslide inventories, Nat. Hazards Earth Syst. Sci. Discuss., 3, 1137–1173, doi:10.5194/nhessd-3-1137-2015, 2015.

Van Den Eeckhaut, M., Vanwalleghem, T., Poesen, J., Govers, G., Verstraeten, G., and Vandekerckhove, L.: Prediction of landslide susceptibility using rare events logistic regression: a case-study in the Flemish Ardennes (Belgium), Geomorphology, 76, 392–410, doi:10.1016/j.geomorph.2005.12.003, 2006.

Van Den Eeckhaut, M., Moeyersons, J., Nyssen, J., Abraha, A., Poesen, J., Haile, M., and Deckers, J.: Spatial patterns of old, deep-seated landslides: a case-study in the northern Ethiopian highlands, Geomorphology, 105, 239–252, doi:10.1016/j.geomorph.2008.09.027, 2009.

Vorpahl P., Elsenbeer H., Marker M., Schroder B.: How can statistical models help to determine driving factors of landslides, Ecological Modelling , 239, 27–39, doi:10.1016/j.ecolmodel.2011.12.007, 2012.

Wang, L.-J., Sawada, K., and Moriguchi, S.: Landslide susceptibility analysis with logistic regression model based on FCM sampling strategy, Comput. Geosci., 57, 81–92, doi:10.1016/j.cageo.2013.04.006, 2013.

Weiss, A.: Topographic position and landforms analysis, ESRI users conference, San Diego, CA, 2001.

Xu, C., Xu, X., Dai, F., and Saraf, A. K.: Comparison of different models for susceptibility mapping of earthquake triggered landslides related with the 2008 Wenchuan earthquake in China, Comput. Geosci., 46, 317–329, doi:10.1016/j.cageo.2012.01.002, 2012.

Yalcin, A., Reis, S., Aydinoglu, A. C., and Yomralioglu, T.: A GIS-based comparative study of frequency ratio, analytical hierarchy process, bivariate statistics and logistics regression methods for landslide susceptibility mapping in Trabzon, NE Turkey, Catena, 85, 274–287, doi:10.1016/j.catena.2011.01.014, 2011.

Yao, X., Tham, L. G., and Dai, F. C.: Landslide susceptibility mapping based on Support Vector Machine: a case study on natural slopes of Hong Kong, China, Geomorphology, 101, 572–582, doi:10.1016/j.geomorph.2008.02.011, 2008.

Yesilnacar, E. and Topal, T.: Landslide susceptibility mapping: a comparison of logistic regression and neural networks methods in a medium scale study, Hendek region (Turkey), Eng. Geol., 79, 251–266, doi:10.1016/j.enggeo.2005.02.002, 2005.

Yilmaz, I.: Landslide susceptibility mapping using frequency ratio, logistic regression, artificial neural networks and their comparison: a case study from Kat landslides (Tokat-Turkey), Comput. Geosci., 35, 1125–1138, doi:10.1016/j.cageo.2008.08.007, 2009.

Zêzere, J. L.: Landslide susceptibility assessment considering landslide typology. A case study in the area north of Lisbon (Portugal), Nat. Hazards Earth Syst. Sci., 2, 73–82, doi:10.5194/nhess-2-73-2002, 2002.

Zhao, C., Lu, Z., Zhang, Q., and de la Fuente, J.: Large-area landslide detection and monitoring with ALOS/PALSAR imagery data over Northern California and Southern Oregon, USA, Remote Sens. Environ., 124, 348–359, doi:10.1016/j.rse.2012.05.025, 2012.

Table 1. Results obtained for the weights of evidence and frequency ratio models.

Factor	Class	FR		WOE		Factor	Class	FR		WOE	
		FR	W+	W−	C			FR	W+	W−	C
1 – Precipitation (mm)	> 833	1.82	0.599	−0.312	0.911	8-Drainage density ($m\,km^{-2}$)	< 1.25	0.892	−0.114	0.009	−0.123
	833–862	1.186	0.170	−0.036	0.206		1.25–1.55	1.534	0.428	−0.094	0.522
	862–882	0.781	−0.247	0.068	−0.315		1.55 – 1.85	1.107	0.101	−0.040	0.141
	> 882	0.448	−0.804	0.298	−1.102		1.85–2.15	0.713	−0.338	0.144	−0.483
							> 2.15	1.024	0.024	−0.005	0.029
2 – Lithology	Clastic (sandstone, siltstone and claystone)	1.799	0.587	−0.030	0.617	9 – Aspect (degree from north)	Flat	0	0.000	0.001	−0.001
	Conglomerate	0.010	−4.571	0.020	−4.590		337.5– −22.5	1.200	0.182	−0.028	0.210
	Gabbro to diorite with ultramafic inclusions	2.195	0.786	−0.009	0.795		22.5– −67.5	2.079	0.732	−0.162	0.894
	Gabbro	0.168	−1.785	0.137	−1.922		67.5– −112.5	2.043	0.715	−0.150	0.865
	Limestone, marble, calc schist and clsstics	1.227	0.204	−0.132	0.336		112.5– −157.5	0.700	−0.356	0.038	−0.394
	Metabasalt and basalt	1.113	0.107	−0.050	0.158		157.5– −202.5	0.211	−1.554	0.105	−1.659
	Ultramafic	1.042	0.41	−0.004	0.045		202.5– −247.5	0.324	−1.127	0.098	−1.225
	Water	0	0	−0.001	0.001		247.5– −292.5	0.523	−0.649	0.074	−0.723
	Flood plain and valley fill sediments	0	0	0.012	−0.012		292.5– −337.5	1.069	0.067	−0.010	0.077
3 – Land cover	Urban and Built-up Land	0	0.000	0.001	−0.001	10 – Curvature (1/m)	< (−3)	0.878	−0.413	0.015	−0.428
	Vegetated Land	0.576	−0.552	0.091	−0.644		(−3)–(−1)	1.012	−0.129	0.020	−0.148
	Cultivated Land	0	0.000	0.000	0.000		(−1)–0	1.044	−0.050	0.016	−0.066
	Burn Land	0.445	0.000	0.000	0.000		0–1	1.028	−0.055	0.034	−0.090
	Harvested Land	1.353	0.302	−0.038	0.340		> 1	0.898	−0.347	0.061	−0.408
	Igneous and/or Metamorphic Rocks	0.934	−0.069	0.052	−0.121	11 – Plan curvature (1/m)	< (−1)	1.01	−0.348	0.030	−0.378
	Sedimentary Rocks	1.279	0.246	−0.110	0.356		(−1)–(−0.5)	1.057	−0.120	0.016	−0.136
4 – Elevation (m)	663–900	1.154	0.143	−0.019	0.162		(−0.5)–0	1.046	0.001	0.000	0.001
	901–1100	1.442	0.366	−0.112	0.478		0–0.5	1.004	−0.043	0.019	−0.062
	1101–1300	0.856	−0.155	0.037	−0.192		0.5–1	0.899	−0.238	0.029	−0.267
	1301–1500	0.259	−1.350	0.156	−1.507		> 1	0.922	−0.437	0.039	−0.476
	1501–1700	0.882	−0.125	0.023	−0.148	12 – Profile curvature (1/m)	< (−1)	0.865	−0.512	0.044	−0.556
	1701–1900	2.118	0.750	−0.118	0.869		(−1)–(−0.5)	0.995	−0.184	0.021	−0.205
	1901–2100	0.527	−0.641	0.020	−0.660		(−0.5)–0	1.055	−0.035	0.011	−0.046
	2101–2360	1.206	0.187	−0.002	0.190		0–0.5	1.02	−0.034	0.015	−0.049
5 – Slope (°)	< 5	0.310	−1.171	0.041	−1.212		0.5–1	1.023	−0.093	0.012	−0.105
	5–10	0.663	−0.411	0.048	−0.459		> 1	0.928	−0.284	0.030	−0.315
	10–15	1.191	0.175	−0.040	0.215	13 – Hypsometric integral	< 0.2	0.144	−1.937	0.047	−1.985
	15–20	1.399	0.336	−0.090	0.426		0.2–0.35	0.838	−0.177	0.024	−0.201
	20–25	1.135	0.127	−0.027	0.154		0.35–0.425	1.705	0.533	−0.235	0.769
	25–30	0.904	−0.101	0.014	−0.116		0.425–0.5	0.952	−0.049	0.025	−0.074
	30–35	0.716	−0.334	0.027	−0.361		0.5–0.6	0.638	−0.450	0.100	−0.551
	> 35	0.933	−0.069	0.006	−0.075		> 0.6	1.168	0.155	−0.003	0.158
6 – Distance to lineaments (m)	< 100	1.165	0.15	−0.021	0.173	14 – TWI	< 6	0.828	−0.188	0.057	−0.245
	100–200	1.052	0.051	−0.007	0.058		6–7	0.919	−0.084	0.013	−0.098
	200–300	1.078	0.075	−0.012	0.087		7–8	1.040	0.039	−0.010	0.050
	300–400	0.893	−0.113	0.016	−0.129		8–9	1.091	0.087	−0.020	0.107
	400–500	0.867	−0.142	0.018	−0.160		9–10	1.064	0.062	−0.008	0.070
	500–750	1.039	0.038	−0.010	0.048		> 10	1.205	0.187	−0.028	0.214
	750–1000	1.287	0.252	−0.033	0.285	15– TPI	< −65	1.123	0.116	−0.036	0.152
	1000–1500	0.585	−0.536	0.026	−0.562		−65–0	1.085	0.082	−0.042	0.124
	> 1500	0.203	−1.596	0.015	−1.611		0–100	1.088	0.084	−0.042	0.127
7 – Distance to drainage (m)	< 100	0.965	−0.036	0.023	−0.059		> 100	0.368	−1.000	0.092	−1.092
	100–200	0.961	−0.040	0.015	−0.055	16 – NDVI	< 0.12	1.105	0.099	−0.026	0.126
	200–300	1.035	0.034	−0.008	0.042		0.12–0.15	1.268	0.238	−0.096	0.333
	300–400	1.322	0.280	−0.035	0.314		0.15–0.18	1.190	0.174	−0.053	0.228
	400–500	0.855	−0.156	0.006	−0.162		0.18 – 0.22	0.730	−0.315	0.052	−0.367
	> 500	0.499	−0.695	0.007	−0.702		> 0.22	0.489	−0.715	0.098	−0.813

Table 2. Results obtained for the probit and logistic regressions models.

Coefficient (X)	(β) Probit estimation	(β) Logistic estimation	Odd ratio of probit	Odd ratio of logistic
(Intercept)	−2.526	−4.233		
HI	0.6125	1.029	1.84	2.8
Slope (°)	0.0012	0.0015	1	1
TWI	0.0229	0.0384	1.02	1.04
NDVI	−3.4	−5.613	0.03	0
Precipitation (mm)	0.0028	0.0047	1	1
Lithology				
Clastic	0.210	0.317	1.28	1.47
Conglomerate	−2.939	−5.894	0.06	0
Gabbro to diorite	−0.767	−1.324	0.48	0.28
Gabbro	−0.769	−1.318	0.49	0.3
Limestone, marble	0.001	−0.006	1.03	1.05
Metabasalt and basalt	−0.341	−0.568	0.73	0.59
Ultramafic	−0.669	−1.107	0.51	0.33
Water	−2.916	−5.864	0.06	0
Flood plain and valley fill	−2.924	−5.873	0.06	0
Aspect (degree from north)				
Flat	−2.117	−4.898	0.07	0
337.5–22.5	0.629	1.014	1.88	2.76
22.5–67.5	0.845	1.374	2.33	3.95
67.5–112.5	0.682	1.102	1.98	3.01
112.5–157.5	0.169	0.271	1.18	1.31
157.5–202.5	−0.316	−0.549	0.73	0.58
202.5–247.5	−0.138	−0.23	0.87	0.79
247.5–292.5	−0.313	−0.546	0.74	0.57
292.5–337.5	0.672	1.093	1.96	2.98

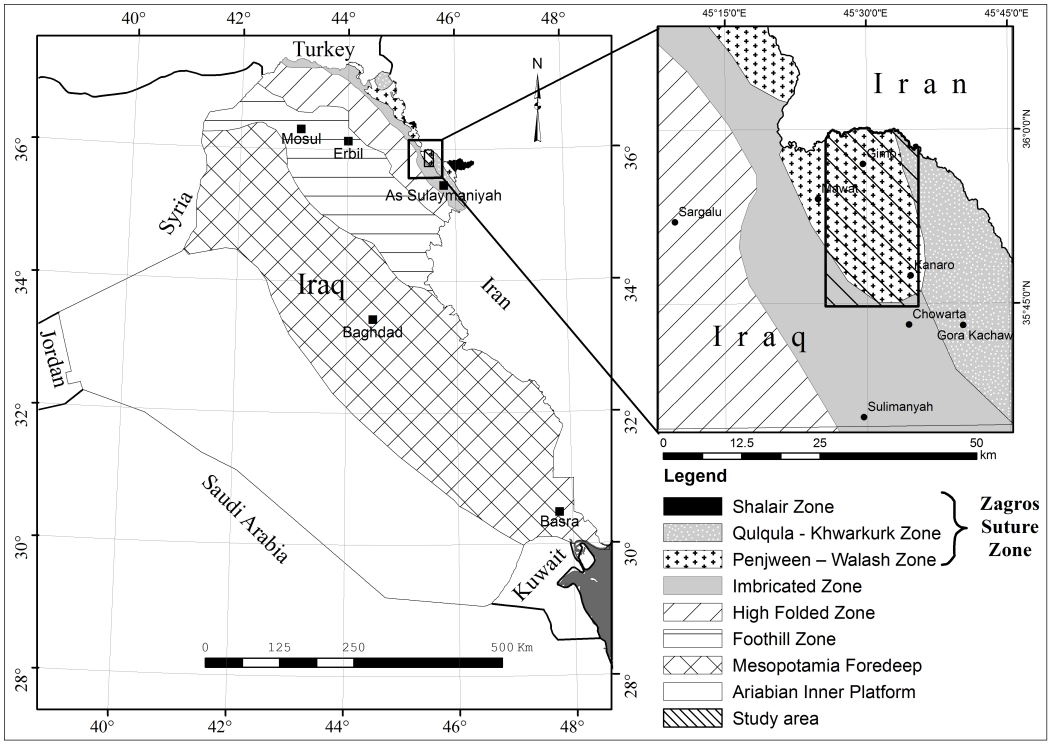

Figure 1. Tectonic map showing the location of the study area which comprises the Imbricated Zone (IZ) and the Zagros Suture Zone (ZSZ) (Fouad, 2010; Jassim and Goff, 2006; Sissakian, 2012).

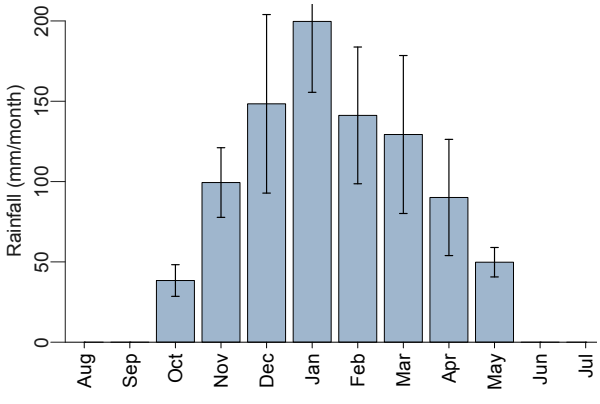

Figure 2. Monthly precipitation in the study area based on data from 2000 to 2006 (the Agro–Meteorological Department of the General Directorate of Research and Agricultural Extension of the Ministry of Agriculture of the Kurdistan Regional Government).

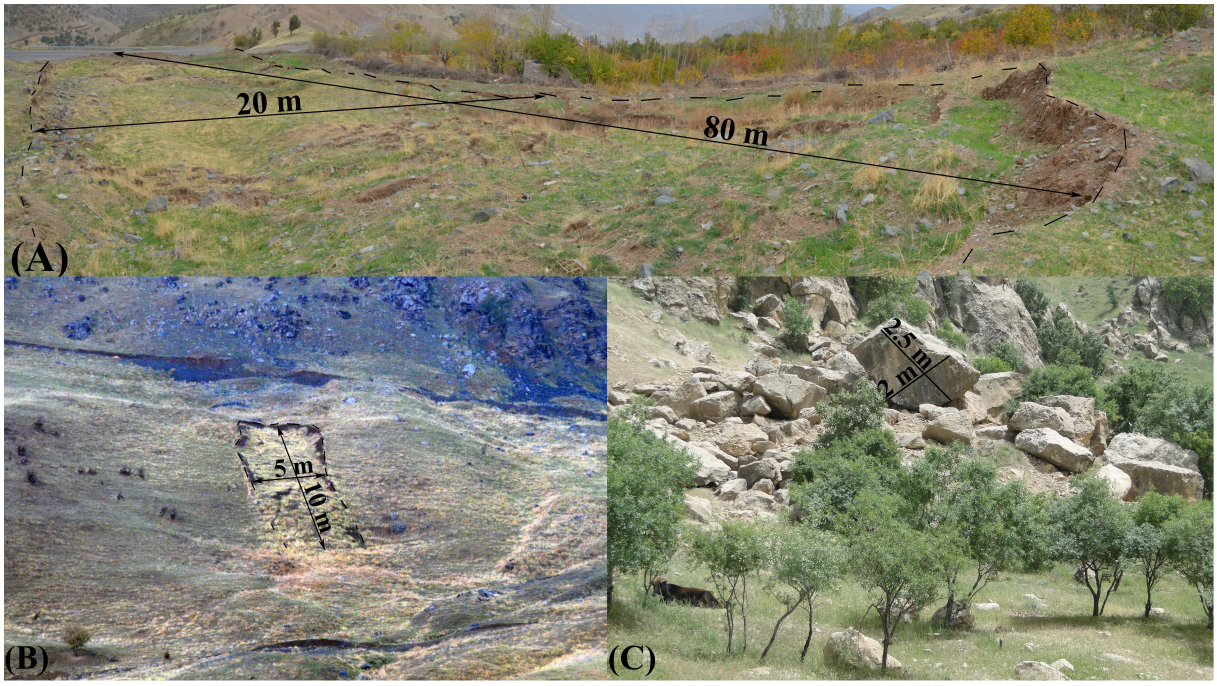

Figure 3. Typical examples of landslides within the study area, where **(A)** panorama of debris slide in the south of Kanaro village; **(B)** debris slide in the south of Basne village; **(C)** rock fall in the north of Chwarta town.

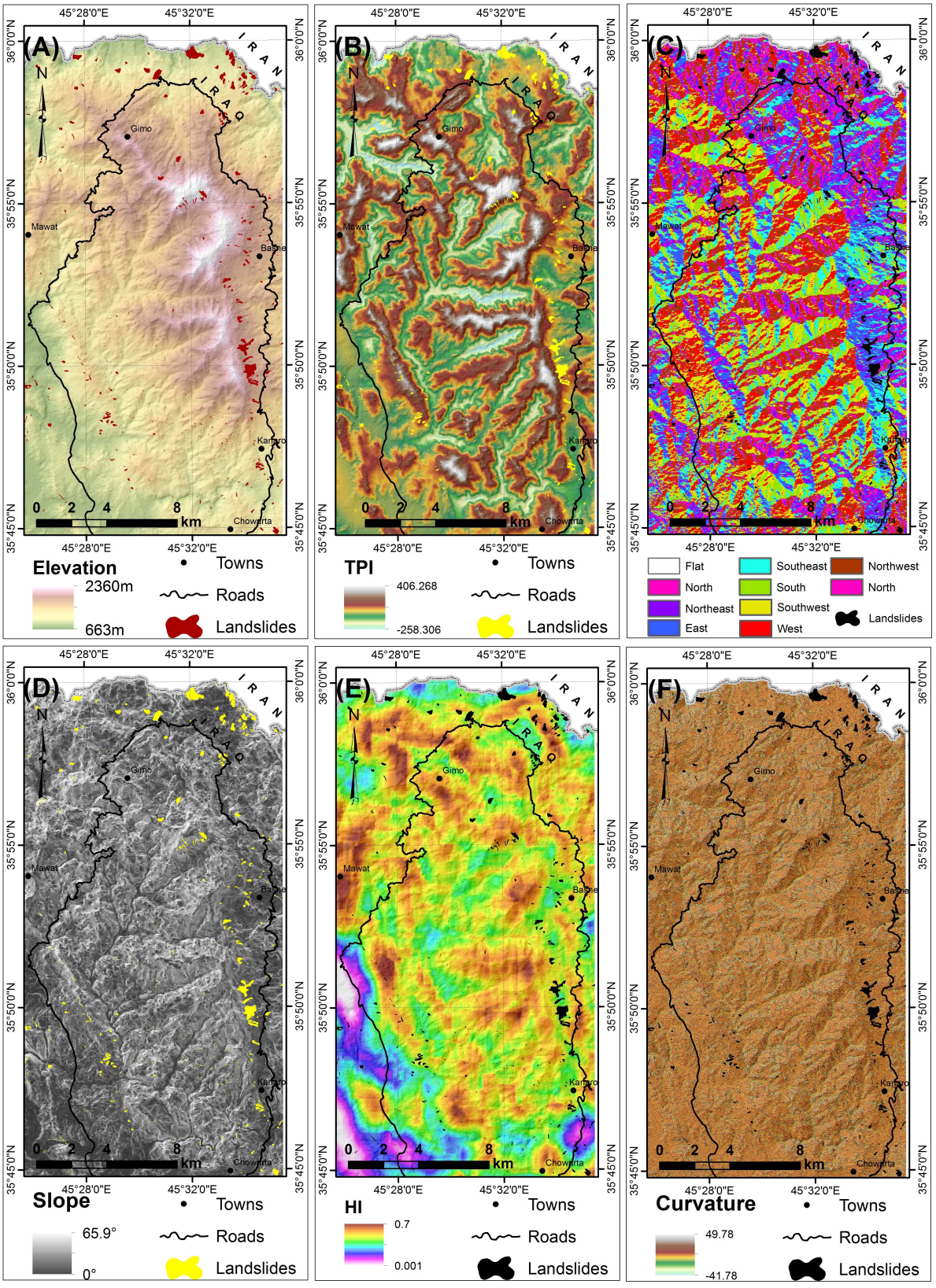

Figure 4. Maps of the landslide geomorphological prediction factors: (A) elevation; (B) TPI; (C) slope aspect; (D) slope angle; (E) HI; (F) curvature.

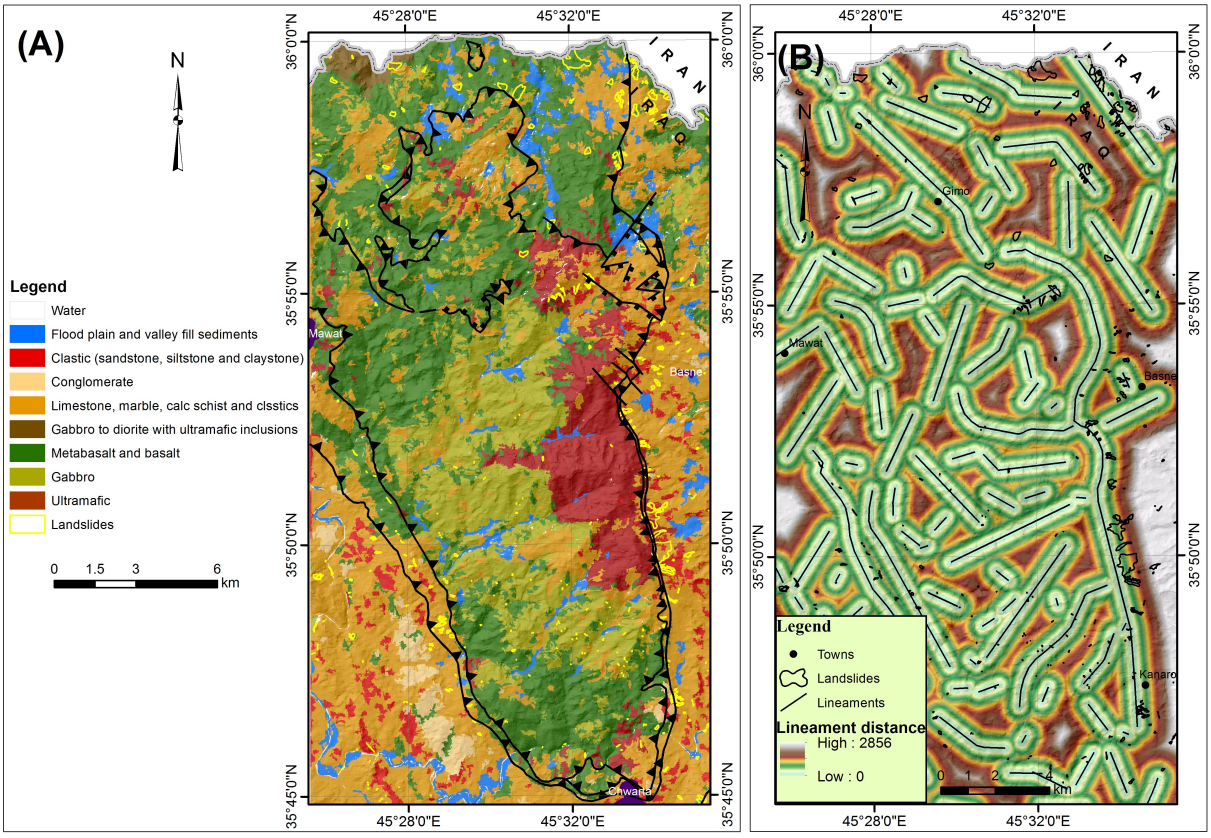

Figure 5. Maps of the landslide geological prediction factors: (A) lithology; (B) distance to lineaments.

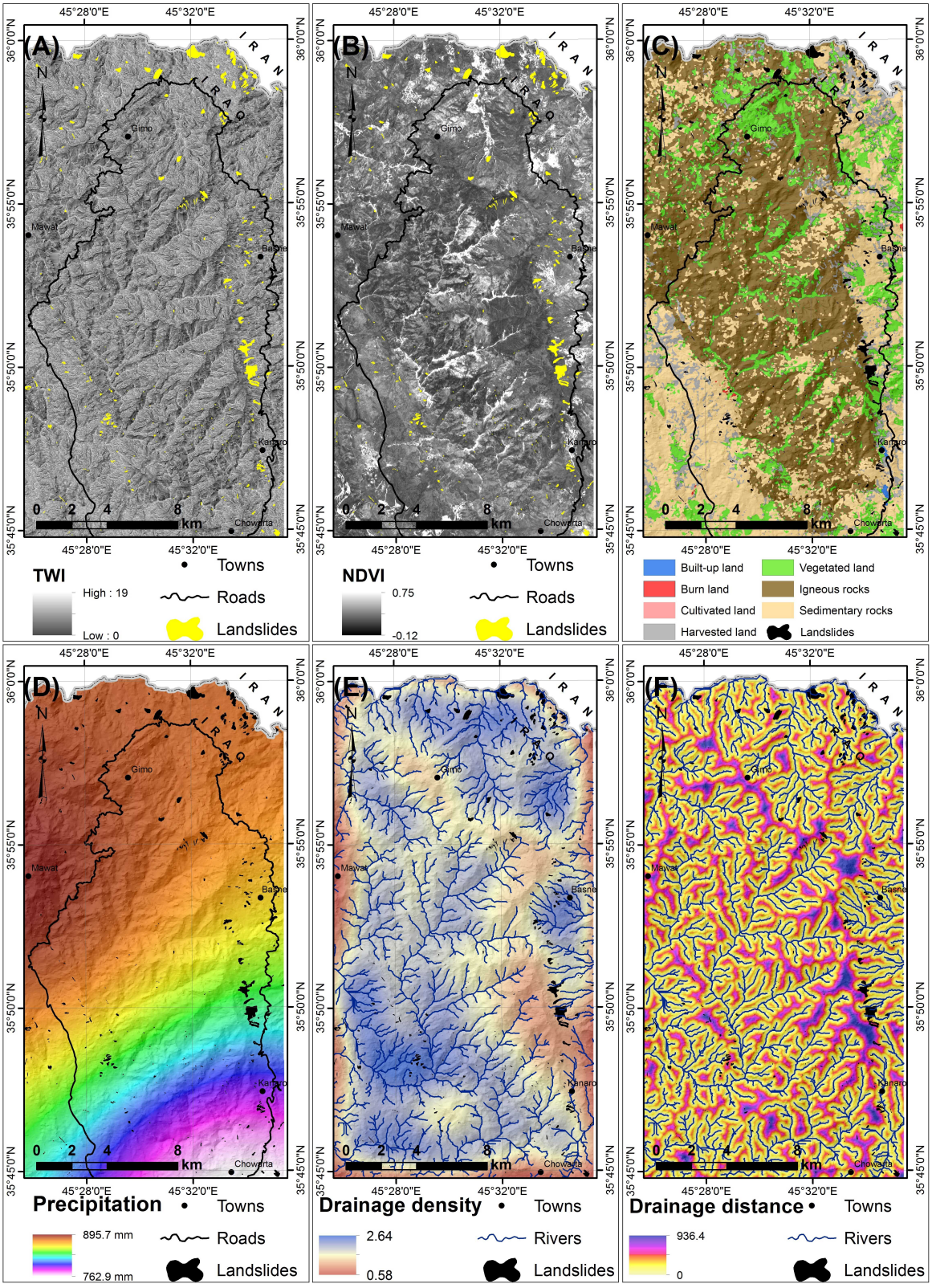

Figure 6. Maps of the landslide environmental prediction factors: (A) TWI; (B) NDVI; (C) land cover; (D) precipitation; (E) drainage density; (F) drainage distance.

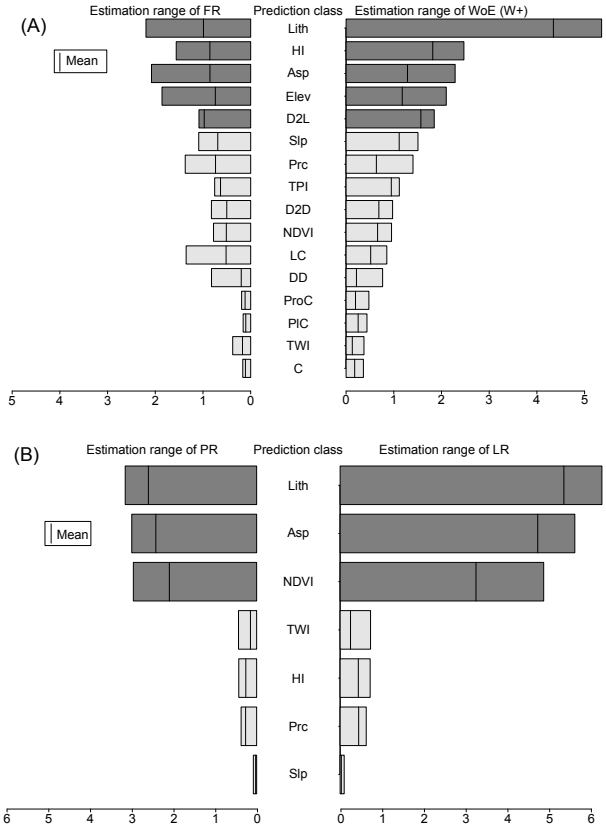

Figure 7. Pyramid plot shows the ranges of the prediction factor estimation weights of (A) weights of evidence and frequency ratio models (B) probit and logistic regressions models. Where, Lith is lithology, HI is hypsometric integral, Asp is aspect, Elev is elevation, D2L is distance to lineaments, Slp is slope, Prc = Precipitation, TPI is topographic position index, D2D is distance to drainage, NDVI is normalized difference vegetation index, LC is land cover, DD is drainage density, ProC is profile curvature, PlC is plan curvature, TWI is topographic wetness index, and C is curvature.

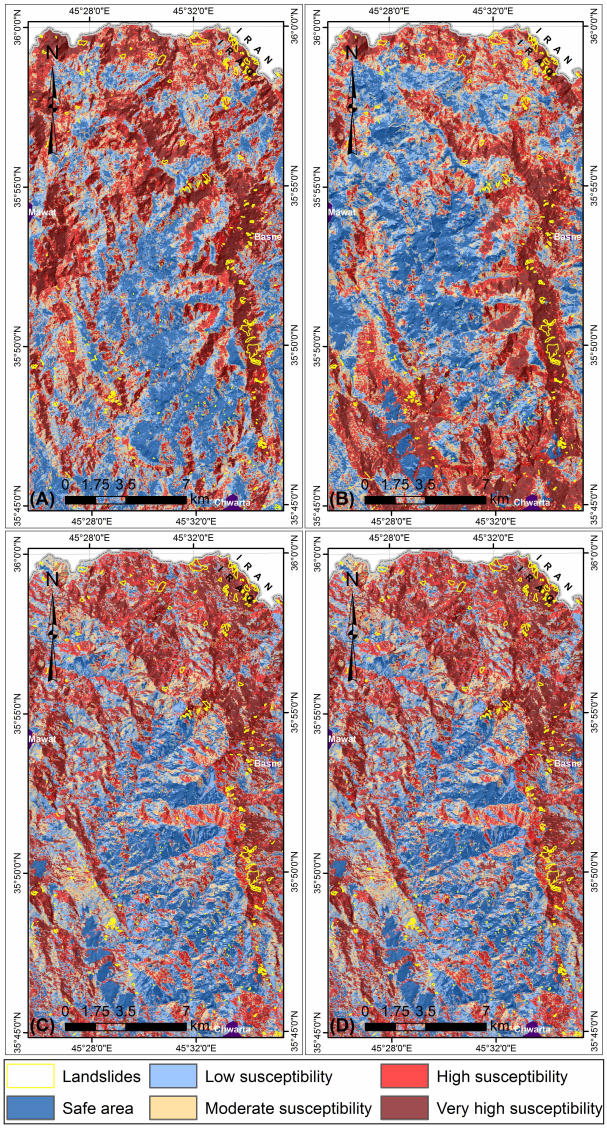

Figure 8. Best spatial distribution of the LS of the study area using: (A) frequency ratio; (B) weights of evidence; (C) logistic regression; and (D) probit regression.

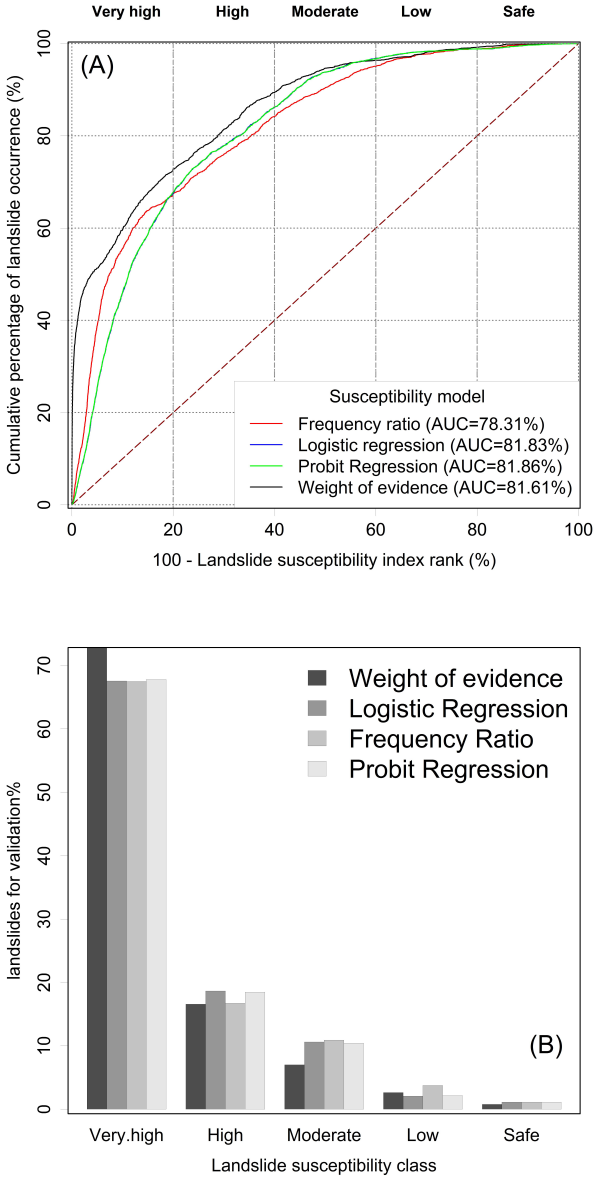

Figure 9. (A) SRC plot evaluation of the four models. LR and PR curves gave similar results and are superimposed. (B) Bar graph showing R–index in different susceptibility classes.

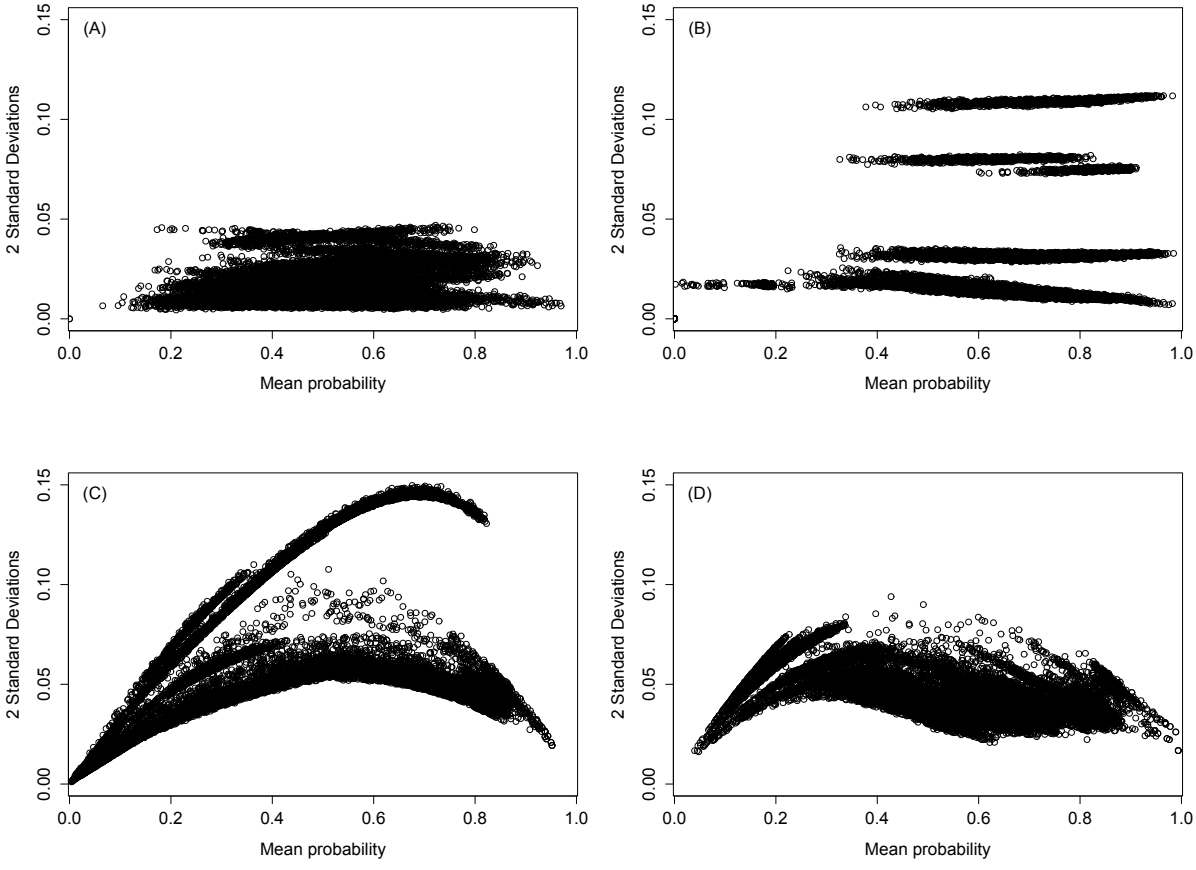

Figure 10. Landslide susceptibility model error. The graphs show the mean value of 50 probability estimates (x-axis) against two standard deviations of the probability estimate (y-axis) for: (A) frequency ratio; (B) weights of evidence; (C) logistic regression; and (D) probit regression.

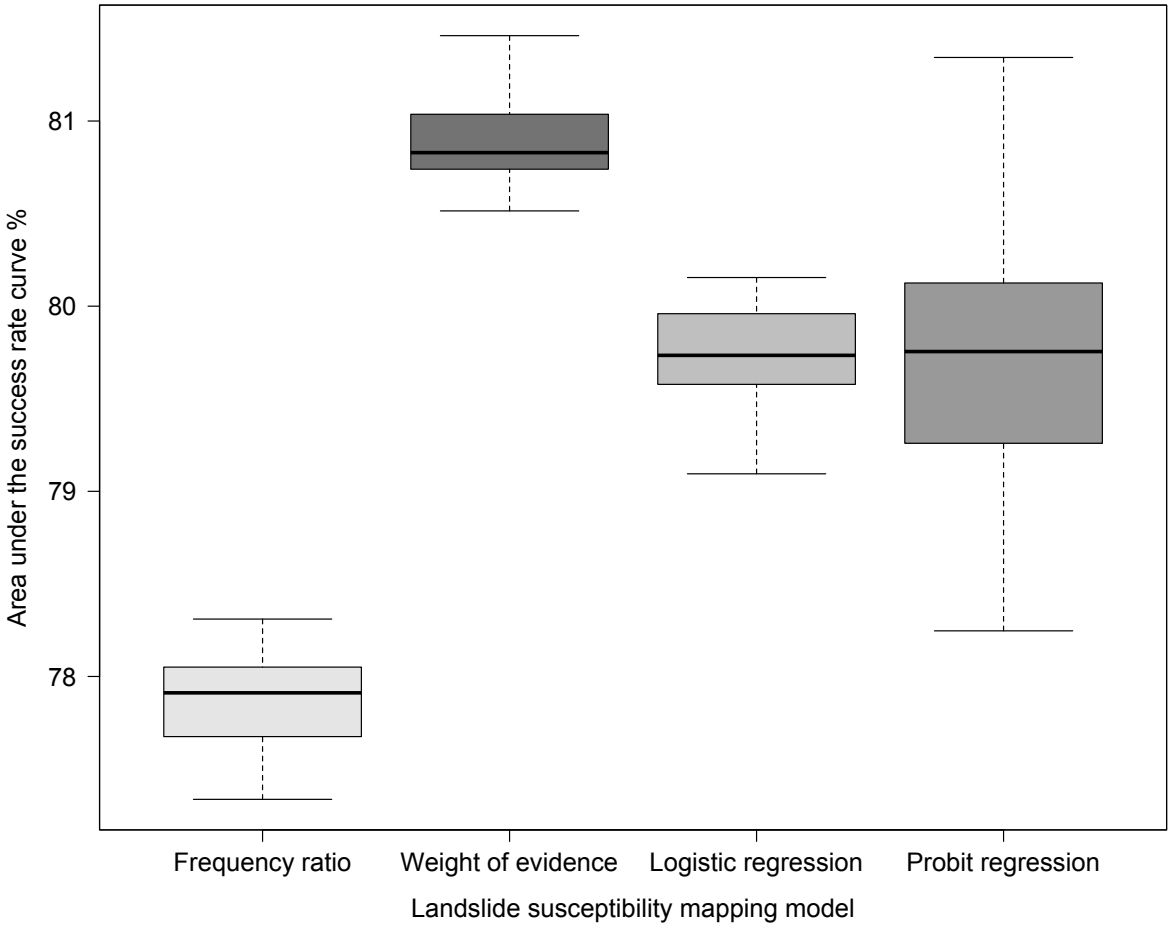

Figure 11. Sensitivity analysis using validation dataset for 50 landslide susceptibility estimates for each of frequency ratio; weights of evidence; logistic regression; and probit regression.